Tungsten impurity transport experiments in Alcator C-Mod to address high priority R&D for ITER

A. Loarte
ITER Organization, Route de Vinon-sur-Verdon, CS 90 046, 13067 St Paul Lez Durance Cedex, France
M.L. Reinke
York Plasma Institute, Department of Physics, University of York, Heslington. York, YO10 5DD, United Kingdom
A.R. Polevoi, M. Hosokawa
ITER Organization, Route de Vinon-sur-Verdon, CS 90 046, 13067 St Paul Lez Durance Cedex, France
M. Chilenski, N. Howard, A. Hubbard, J.W. Hughes, J.E. Rice, J. Walk and the Alcator C-Mod Team
Plasma Science and Fusion Center, Massachusetts Institute of Technology, Cambridge, Massachusetts 02139, USA.
F. Köchl
Technische Universität Wien, Atominstitut, Stadionallee 2, 1020 Vienna, Austria
T. Pütterich, R. Dux
Max-Planck-Institut für Plasmaphysik, Boltzmanstraβe 2, D-85748 Garching, Germany
V. E. Zhogolev
NRC "Kurchatov Institute", Kurchatov square 1, 123098 Moscow, Russia

Abstract. Experiments in Alcator C-Mod tokamak plasmas in the Enhanced D-alpha (EDA) H-mode regime with ITER-like mid-radius plasma density peaking and Ion Cyclotron Resonant heating (ICRH), in which tungsten is introduced by the laser blow-off technique, have demonstrated that accumulation of tungsten in the central region of the plasma does not take place in these conditions. The measurements obtained are consistent with anomalous transport dominating tungsten transport except in the central region of the plasma where tungsten transport is neoclassical, as previously observed in other devices with dominant neutral beam injection heating such as JET and ASDEX Upgrade. In contrast to such results, however, the measured scale lengths for plasma temperature and density in the central region of these Alcator C-Mod plasmas, with density profiles relatively flat in the core region due to the lack of core fuelling, are favourable to prevent inter and intra sawtooth tungsten

accumulation in this region under dominance of neoclassical transport. Simulations of ITER H-mode plasmas including both anomalous (modelled by the Gyro-Landau-Fluid code GLF23) and neoclassical transport for main ions and tungsten and with density profiles of similar peaking to those obtained in Alcator C-Mod show that accumulation of tungsten in the central plasma region is also unlikely to occur in stationary ITER H-mode plasmas due to the low fuelling source by the neutral beam injection (injection energy ~ 1MeV), which is in good agreement with findings in the Alcator C-Mod experiments.

1. Introduction.

The next generation of fusion devices, such as ITER, is expected to operate with tungsten (W) plasma facing components (PFCs) and in regimes with high energy confinement in order to demonstrate high fusion power amplification [1]. Due to its high electronic charge, W remains partially ionized in the plasma, even for the range of temperatures expected in the central region of the plasma in ITER (T_e ~ 10-30 keV), thus causing large radiative power losses from the plasma by line emission of the partially ionized W atoms excited by electron impact. As a consequence, the concentrations of W in the confined plasmas which are compatible with high energy confinement and high fusion power amplification in nuclear fusion reactors are very low (typically few 10^{-5}) [2]. The need to control the concentration of W in the confined plasma is not restricted to next step fusion devices but it is already required for present tokamak experiments. Lack of W concentration control causes the radiated losses from the plasma to approach or exceed the plasma heating power, which triggers MHD instabilities that usually end up in a disruption [3].

Operation in the H-mode high energy confinement regime is more challenging from the W concentration control point of view due to the formation of a region with very low anomalous transport at the plasma edge (edge transport barrier or ETB). In the ETB impurity transport is found to be well described by neoclassical transport for low-Z to mid-Z impurities [4] which, for typical edge density and temperature profiles in present experiments, has an inward convective velocity component [5]. This leads to peaked W profiles in the ETB region with values of the W concentration in the inner part of the ETB much larger than those near the plasma separatrix. Production of W by sputtering of the PFCs together with the unfavourable transport in the ETB can lead to the uncontrolled increase of the W concentration in the edge of the confined plasma in the absence of other processes. This edge W concentration increase is arrested by the occurrence of edge MHD instabilities (ELMs) which cause an expulsion of particles from the edge plasma or by enhanced edge turbulence observed in H-mode regimes which either do not have ELMs such as the EDA (Enhanced D-alpha) H-mode confinement regime [6] or in which 3-D magnetic field perturbations are applied to supress them [7]. Control of ELMs and of the divertor W erosion source between the ELMs is expected to be appropriate to provide the required level of W concentration control in the region of the ETB in ITER [8].

The control of the W concentration to an acceptable level in the edge plasma region in H-modes is a necessary but not sufficient condition to ensure that the concentration of W in the central region of the plasma remains low enough to prevent excessive radiation, which

leads to the termination of the high confinement H-mode regime. Uncontrolled increases of the core W concentration (for quasi-stationary values of the edge W concentration) are frequently observed for H-mode discharges in tokamaks operating with W PFCs whose plasma heating is dominated by neutral beam injection (NBI) [9]. The physics picture recently demonstrated to explain this phenomenology in H-mode plasmas is that W transport is dominated by anomalous transport for most of the plasma cross section inside the ETB except the very central region close to the magnetic axis [10, 11, 12]. In this central region W anomalous transport is negligible and W transport is dominated by neoclassical effects, similar to earlier ASDEX Upgrade observations using extrinsic seeding of noble gases [13]. Therefore, peaking of the W density in the central plasma region is determined by the competition between the ion density radial gradient (which produces an inward W flux) and the ion temperature radial gradient (which produces an outwards W flux usually called temperature screening). In experiments with dominant NBI heating the ion density and temperature gradients are often such that their net effect is to drive a significant inward flow leading to strong peaking of the W density profile [11]. An important factor in this behaviour is the fact that NBI heating unavoidably provides a source of neutrals in the central plasma region thus leading to a sizeable peaking of the ion density profile there [14]. This relation between the ion density and temperature gradients in the central region of the plasma for NBI dominated plasmas can be modified by the application of central RF heating (ECRH and ICRH) thus avoiding an uncontrolled increase of the core W density [9, 15]. This picture is complicated by the role that these additional heating systems play in sustaining poloidal variations in high-Z impurity density, which is shown to have an important impact on the flux-surface averaged neoclassical radial impurity transport [16]. Sustained MHD activity [10, 11] may also complicate this picture, but experiments and simulations discussed here focus on plasmas that are MHD-free or have resolvable, discrete MHD events (i.e. sawteeth).

Despite the wide range of experimental results regarding W density peaking in the central plasma described above, their implications for ITER remain uncertain. This is due to differences between ITER and present experiments beyond those associated with the larger device size and plasma parameters (which may lead to different physics processes dominating plasma transport), such as:

a) heating schemes, which are dominated by electron heating in ITER versus present experiments most of which are ion heating dominated.

b) central plasma fuelling, whose rate is typically one order of magnitude or more smaller in ITER than in present experiments due to the high energy of the NBI injected

particles (~1 MeV in ITER versus 50-100 keV in present experiments). When the plasma volume is taken into account, the fuelling rate per unit volume in the central plasma of ITER is typically two to three orders of magnitude smaller than in present experiments

c) plasma toroidal rotation which is expected to have a low Mach number in ITER (in the absence of large intrinsic rotation) due to the lower momentum input by the NBI due to their higher injection energy.

d) The interaction between toroidal rotation and impurity transport, as impurity toroidal rotation is known to affect impurity transport [11, 12, 16].

All these factors together with differences in the underlying shape of the plasma density and temperature profiles between present experiments and ITER, which influence W transport, make impossible a straightforward extrapolation of the present experimental results to ITER.

This paper describes the results of modelling studies of W transport for ITER reference operational conditions and the results of a series of experiments on the Alcator C-Mod tokamak to characterize W transport in conditions similar to those expected in ITER in terms of: a) core electron density and ion and electron temperature peaking, b) plasma toroidal rotation, c) dominant electron heating and d) low/no source of neutrals injected by the heating systems in the plasma central region.

The paper is organised as follows: section 2 summarizes the results of the modelling studies of W transport for the reference 15MA/5.3T high fusion gain Q_{DT} =10 scenario in ITER, section 3 describes plasma conditions and experimental techniques utilized to characterize W transport in the Alcator C-Mod experiments, section 4 describes the results concerning W transport in Alcator C-Mod and its dependencies on discharge parameters and finally section 5 summarises the results in view of their extrapolation to ITER, draws conclusions and discusses future directions for Alcator C-Mod R&D in this area.

2. Modelling of W transport in ITER.

Modelling of W transport for the ITER core plasma has been carried out with the ASTRA modelling code, which includes a model for anomalous main ion and W transport based on the GLF23 transport model [17, 18]. In addition to anomalous transport, neoclassical transport is evaluated with transport coefficients obtained from the NCLASS code [19] for main ions and W impurities. Impurity transport is modelled by the code ZIMPUR [20] which is coupled to the main plasma ion transport in ASTRA. In all the simulations performed for ITER the value of the W density at the plasma edge is set as a boundary conditions with low concentration values ($< 10^{-5}$) so that the W radiative losses from the main plasma are low and do not affect the core plasma parameters. This is appropriate for the purpose of these studies

as they focus on the determination of whether the W density profile will be strongly peaked with respect to the main ion density profile in ITER or not. The evaluation of the expected W level in ITER requires more sophisticated modelling including the effect of controlled ELMs on W expulsion and production of W by sputtering from the divertor and its transport in the scrape-off layer (SOL), which is beyond the scope of this paper. The modelling assumptions are thus:

- Plasma conditions in the ETB region are evaluated by predictions of the EPED model [21] and used as boundary conditions for the studies of core plasma transport
- Energy and particle transport for main ions and W is provided by the sum of the contributions from anomalous transport (evaluated with the GLF23 model) and neoclassical transport evaluated with NCLASS so that:
    - $\chi_{e,i} = \chi_{i\text{-neo}} + \chi_{e,i\text{-GLF}}$
    - $D_{i,W} = D_{i,W\text{-neo}} + D_{i.W\text{-GLF}}$
    - $V_{i,W} = V_{i,W\text{-neo}} + V_{i,W\text{-GLF}}$
    - $\chi_{momentum} = \chi_{i\text{-neo}} + Pr \times \chi_{i\text{-GLF}}$

where subscripts with the neo suffix refers to the values evaluated on the basis of neoclassical transport and the GLF suffix refers to those from anomalous transport, χ_e and χ_i are the heat diffusivities for electrons and main ions respectively, $D_{i,W}$ and $V_{i,W}$ are the particle diffusivities and particle velocity pinches for the main ions and W respectively, and $\chi_{momentum}$ is the momentum diffusivity for the main ions and Pr is the Prandtl number. It should be noted that this approach to model toroidal rotation is rather simplistic and leads to relatively low toroidal Mach numbers being predicted for ITER for Pr ~ 1, given the low momentum source from the NBI and the fact that no intrinsic rotation is included in these simulations. Similarly, including a sizeable momentum pinch could change these results significantly affecting, among other plasma parameters, impurity transport as it will be discussed later. The value of the E×B shear amplification factor α_E used in the GLF23 linear turbulence quench rule is taken to be $\alpha_E = 1$ in these simulations. For the electrons the value of heat diffusivity when anomalous transport is negligible is set to that of ion neoclassical transport; otherwise the very low value of the electron neoclassical thermal diffusivity ($\chi_{e\text{-neo}} \sim 1/60 \times \chi_{i\text{-neo}}$) leads to unphysical high electron temperatures in the simulations. This reflects the fact that reduction of electron and ion turbulent heat transport under the level of ion neoclassical heat transport predictions is not commonly observed in experiments (for instance, in the ETB

electron and ion heat transport are commonly observed to reduce to levels of ion neoclassical heat transport, which is a factor of ~ 60 higher than electron neoclassical heat transport).

ITER simulations have been carried out for the ITER DT plasmas in stationary phases of the reference high fusion gain scenario (Q_{DT}=10) with plasma current of 15 MA and toroidal field of 5.3 T and for a lower current/toroidal field plasma (7.5 MA/2.65 T), representing typical low current plasmas in which initial H-mode operation will be developed in DT in ITER. For both cases additional heating power of ~ 50-53 MW has been applied with 33 MW of NBI heating and the remaining 17-20 MW from radiofrequency heating (ICRH or ECRH). It should be noted that in the ITER reference high Q_{DT} scenario the dominant plasma heating (~ 100 MW) is provided by alpha particles produced by the fusion reactions which thermalize in the plasma. The results regarding plasma W transport in both ITER scenarios are qualitatively similar; thus we only will describe in detail the studies for the 15 MA/5.3 T plasma as this is more relevant regarding the achievement of ITER mission's and for fusion tokamak reactors in general.

The plasma parameters obtained for a range of simulations for the ITER 15 MA/5.3 T Q_{DT} ~10 plasma applying different heating schemes (33 MW of NBI + 20 MW of off axis or on axis ECRH and 33 MW of NBI + 20 MW of on axis ICRH with He^3 minority to provide maximum ion heating) are shown in Fig. 1 a-d. As previously identified, for the typical conditions expected in ITER the plasma density profile is moderately peaked $n_i(0)/n_{i\text{-}ped}$ ~ 1.6 despite the low level of core NBI fuelling, which is in good agreement with expectations for ITER on the basis of experimental data for low collisionality H-modes [22]. This is due to the existence of an anomalous inwards particle pinch over most of the cross section of the ITER plasma in the GLF23 modelling. It should be noted that in these simulations the Prandtl number has been varied (within the same range for all simulations) in a range of Pr = 0.2 - 1.0, which leads to a ratio of momentum (τ_ϕ) to energy confinement (τ_E) times of τ_ϕ/τ_E = 0.3 - 1.0. For these values of the Prandtl number the plasma thermal energy agrees with expectations from the ITER-98 energy confinement time scaling law (i.e. H_{98} = 1) [23] leading to a fusion performance of Q_{DT} ~ 10 for the expected values of the pedestal pressure in the ETB predicted by the EPED model [21]. In our modelling the value of the Prandtl number affects toroidal rotation shear, which in turn affects the stiffness of the ion temperature profile predicted by the GLF23 model and the predicted fusion performance. It is well known that, without inclusion of rotational shear effects weakening the ion temperature stiffness and with a pedestal pressure value in agreement with the EPED model, the

anomalous transport from the GLF23 model predicts a fusion performance for ITER 15 MA/5.3T plasmas of Q_{DT} ~ 6-7 [24].

The predicted W density profiles and anomalous W transport for these three ITER simulations are shown in Fig. 2.a-b. As can be seen in Fig.2.a the W density profiles are flat over most of the plasma cross section and in the central part they can be somewhat peaked but with similar $n_W(0)/n_{W\text{-}ped}$ to $n_i(0)/n_{i\text{-}ped}$ or lower and thus similar W concentration across the plasma cross section. Of the three cases considered, the one with the highest W peaking is that with off-axis ECRH heating. The physics processes that lead to this W density profile shapes can be understood from Fig.2.b. For these plasma conditions W transport is found to be dominated by anomalous transport over most of the plasma cross section (r > 0.25-0.4 m) with a large diffusion coefficient (shown in Fig. 2.b) and very low anomalous pinch (not shown). In the very central part of the plasma (r < 0.25-0.4 m) anomalous transport is negligible and neoclassical W transport dominates. Thus whether W is more or less peaked in this region depends on the relative scale lengths of the ion density and temperature profiles in this region. Application of central heating (whether pure electron heating with ECRH or mixed ion-electron heating with He^3 minority ICRH heating) changes the relative scales of the ion density and temperature profile in this region and correspondingly decreases the central values of the W density (see Fig. 3), as the intensity of temperature screening increases with respect to the inward flux driven by the ion density gradient. It should be noted that in the simulations the effect of central electron heating and ion heating are different although they produce a similar result regarding W transport. Central electron heating increases the ion density scale length (at ~ constant ion temperature scale length) while ion heating decreases the ion temperature scale length (at ~ constant electron and ion density scale lengths). This is somewhat different from results on ASDEX-U which showed ECRH and ICRH both reducing the W peaking, but the former through increasing W anomalous diffusion and the later through reduced inward neoclassical convection [25].

The effectiveness of central RF heating (P_{RF} = 20 MW) to affect the main ion temperature and density profiles despite the dominance of alpha heating (P_α = 100 MW) can be understood because of the much more peaked power deposition profiles of the heating provided by RF than by alpha heating. Table 1 shows the calculated power densities in electron and ions for the two cases for ITER plasmas with 15 MA/5.3T – Q_{DT} = 10 with central RF heating described above. From the values in this table it is clear that the ITER RF heating systems have the capabilities to increase the power density in the central region which is deposited in the electrons by a factor of 2-3 above that of the value from alpha heating and

for the ions by up to a factor of 2, despite the integral heating power from alpha heating being five times higher than that of the RF one. If the temperatures profiles are non-stiff in the core region this will lead to a decrease of the temperature scale length (improved temperature screening seen for central ICRH heating in Fig. 3). If, on the contrary, the temperature profiles are very stiff in this central region this will lead to no change in the temperature profile but to an increase of anomalous transport that flattens the density profile (reduced inward W transport seen for central ECRH heating in Fig. 3).

The results of these modelling studies for ITER are in excellent qualitative agreement with recent studies of W transport and W peaking in JET experiments [11, 12] and its control by ICRH heating (electron heating) [15]. These studies also find that large diffusive anomalous W transport dominates inside the ETB except for the very central region of the plasma where W transport is neoclassical. In agreement with these studies the ITER simulations only find indications of central peaking in the W density profile when

$$\frac{a}{L_{n_i}} - \frac{a}{CL_{T_i}} >> 0 \qquad (1)$$

where C ~ 2.5-2.8 for ITER and C ~ 2 for present experiments, -i.e. for the case with off-axis ECRH heating. It should be noted that, due to the lower collisionality of W in the ITER plasmas compared to present experiments, the contribution of banana-plateau transport in the core of ITER plasmas to the W neoclassical transport is significant (it accounts for 50% of the value of the diffusion coefficient in the central plasma region). This affects the strength of temperature screening by decreasing the temperature screening factor from the usual H ~ 0.5 (leading to C ~ 2 in Eq. (1)) in present experiments [11, 12], where W transport is dominated by Pfirsch-Schlüter transport, to H =0.35-0.4 (leading to C ~ 2.5 – 2.8 in Eq. (1)) for ITER [26].

Despite these qualitative similarities, there are significant quantitative differences between the predicted W transport in ITER and in these JET experiments. Some of them are linked to the low values of plasma rotation in these ITER simulations ($M_{DT} \leq 0.1$ for the simulations with Pr = 0.2 and $M_{DT} \leq 0.03$ for the simulations with Pr = 1.0) compared to those of JET (M_{DT} ~ 0.4) [11], which can strongly increase the magnitude of the neoclassical transport coefficients for W due to centrifugal effects. To quantify the effect of toroidal rotation on W poloidal asymmetries and on the ensuing neoclassical transport in these ITER plasma conditions, we have performed modelling studies with the NEO code [27]. In these studies we have scanned the toroidal rotation frequency so that M_{DT} covers the range from the values in our ITER simulations (M_{DT} = 0.05) to the values measured in experiments (M_{DT} = 0.4), while keeping

the plasma density and temperature profiles constant (the case with off-axis ECRH heating in Figs. 1 and 2 has been considered). The results of this study are shown in Fig. 4. In this figure the results of NEO modelling (for W^{63+}, a typical ionization state of W in the plasma centre in these ITER conditions) and NCLASS (including a range of W ionization stages evaluated by the transport code ZIMPUR) are compared. For the low Mach numbers in our simulations centrifugal effects on W neoclassical transport are very small and the agreement between NEO and NCLASS is very good, consistent with previous studies [11]. On the other hand, for $M_{DT} \geq 0.2$ there are significant differences between NCLASS and NEO predictions with D_W and V_W increasing as the Mach number increases, as predicted by neoclassical transport effects for poloidally asymmetric impurity density profiles [16], while keeping a similar ratio V_W/D_W (i.e. a similar peaking of the W profile in stationary conditions). It is interesting to note that for the highest Mach number, $M_{DT} = 0.4$, the direction of the neoclassical pinch can change sign due to toroidal rotation and the associated poloidally asymmetric impurity density profiles, as already pointed out in [12]. On the basis of these results we conclude that, for a large range of toroidal rotation velocities, toroidal rotation effects in ITER can strongly affect the timescale on which the W profiles develop to stationary conditions (increased D_W with M_{DT}) but not strongly affect the stationary peaking of these profiles (similar V_W/D_W for a range of M_{DT}). At the largest Mach numbers considered ($M_{DT} = 0.4$) the effects on W neoclassical transport are more significant and the stationary W profiles expected in ITER would be less peaked (even hollow) in the plasma centre than those obtained in our simulations (with NCLASS) that do not include these effects.

Other quantitative differences are linked to the magnitude of the central source provided in ITER by the neutral beam injection compared to the ion heating power density and to its implications for the ratio of the ion density and temperature scale lengths in the core plasma region, which is given by:

$$\frac{L_{n_i}}{L_{T_i}} = \frac{D_i q_i}{\chi_i \Gamma_i T_i} \qquad (2)$$

Taking into account the central plasma conditions in the ITER Q_{DT} =10 plasmas ($q_i \sim 0.35$ MWm^{-3}, $\Gamma_i \sim 3\ 10^{17}$ $m^{-3}s^{-1}$,$T_i \sim 20$ keV) and those of the JET plasmas in [11] plasmas ($q_i \sim 0.6$ MWm^{-3}, $\Gamma_i \sim 7\ 10^{19}$ $m^{-3}s^{-1}$,$T_i \sim 5$ keV) and assuming that in the central plasma region D_i/χ_i is independent of device size (this is the case for neoclassical transport) leads to:

$$\frac{\left.L_{n_i}/L_{T_i}\right|_{JET}}{\left.L_{n_i}/L_{T_i}\right|_{ITER}} = \frac{q_i^{JET}}{q_i^{ITER}} \frac{\Gamma_i^{ITER} T_i^{ITER}}{\Gamma_i^{JET} T_i^{JET}} \sim 0.03 \quad (3)$$

showing a clear trend for the ion density profiles to be much more peaked relative to the ion temperature profiles in the JET experiments in [11] than those for typical ITER Q_{DT} = 10. The JET and ASDEX Upgrade NBI-dominated experiments are thus in a situation more prone to core W accumulation than ITER Q_{DT} = 10 plasmas.

While these modelling results and considerations for ITER are very encouraging for the situation concerning W transport in the core plasma of ITER, significant uncertainties remain regarding the modelling results, such as:

a) the accuracy with which any model for anomalous transport can predict the gradients for density and temperature in the region where anomalous transport is dominant.

b) the extent of the region in the plasma centre in which anomalous transport is low.

c) the level of residual electron transport in this central region.

d) the role of sawteeth in affecting W transport. Although initial ITER simulations including the effect of sawteeth do not show a different qualitative picture that when they are not included for ITER, the model for W expulsion by sawteeth as well as the recovery of the plasma density and temperature following the sawteeth are subject to modelling uncertainties due to the large gradients that can be transiently formed.

e) The level of toroidal plasma rotation in ITER and its effect on W transport.

Therefore, it is required to validate if the positive trends regarding W transport in the core plasma identified in the ITER modelling are indeed found in the experiment. For this purpose a series of experiments was carried out in the Alcator C-Mod tokamak to characterize W transport in conditions that match specific aspects of the ITER plasmas which have been found by modelling to have significant effects on W transport in the core plasma.

3. Overview of experiments in Alcator C-Mod.

Alcator C-Mod [28, 29] is a compact, high field tokamak with vertical plate divertor geometry and RF-based heating and current-drive systems (LHCD and ICRH). The experiments reported in this paper were carried out with central ICRH heating of plasmas in the EDA H-mode confinement regime [6]. The EDA H-mode is an ELM-less H-mode plasma in which density transport is enhanced by the presence of a quasi-coherent mode at the plasma

edge which arrests the density rise typical of ELM-free H-mode and prevents the uncontrolled increase of impurities in the core that would otherwise lead to excessive bulk plasma radiation even in the absence of a large core impurity peaking [5, 30, 31, 32]. Steady high performance EDA H-modes have similar pedestal pressure profiles to those obtained in ELM-free H-modes [33], and only a slight reduction in maximum normalised energy confinement results from the EDA onset [6].

The quasi-coherent mode also prevents the plasma from reaching unstable edge pressure/current gradients and thus triggering edge instabilities known as ELMs. Because of the large erosion of ITER PFCs [34] and the detrimental effects on plasma performance of impurity influxes produced by ELMs, the maximum loss of energy during ELMs must be significantly reduced in ITER from its expected "natural" or "uncontrolled" values by large factors (typically ~ 30 for Q_{DT} =10 plasmas) by controlled triggering of ELMs [8]. Controlled ELMs are also required to provide appropriate W exhaust from the confined plasma in ITER even for conditions in which uncontrolled ELMs would be acceptable from the divertor erosion point of view [8]. In this respect, the EDA regime in Alcator C-Mod represents a good proxy for the controlled ELM regimes required in ITER.

The experiments described in this paper were carried out with a plasma current of 0.44-0.6 MA and a toroidal field of 5.4 T, corresponding to q_{95} = 6 – 8, with the ion grad-B direction favourable for H-mode access in a lower single null diverted plasma configuration. All discharges were heated by ICRH and the ICRH heating power into the plasma spanned the range from 1.0 – 3.6 MW. The lower limit was dictated by access to the H-mode regime while the upper limit was defined either by the maximum ICRH power that could be reliably coupled to the plasma (for 0.6 MA) or by acceptable loads at the limiters from ions accelerated by the ICRH (for plasma currents of 0.44 and 0.52 MA). The plasma line average density normalized to the Greenwald limit was typically $\langle n_e \rangle / n_{GW}$ ~ 0.3-0.4 in these experiments and the effective plasma collisionality was $1.0 < \nu_{EFF} < 4.0$ [22]. These relatively low current/high q_{95} (much larger than for Q_{DT} = 10 operation in ITER) and high ICRH heating power plasmas were chosen to perform these experiments on W transport characterization in Alcator C-Mod because the density peaking obtained in them is similar to that expected in ITER for H-mode operation [35] and because density peaking is a key factor driving core W accumulation in present experiments and ITER. Other important features of these experiments regarding their possible effect on W transport which are similar to ITER are:

- Dominant electron heating (typically q_e/q_i ~ 2-3) provided by the ICRH H-minority heating scheme, similar to typical ratios in ITER, and with peaked deposition profiles (typically, the deposited ICRH power density profile is peaked at r/a = 0.1-0.15 and most of the ICRH power is deposited within r/a ≤ 0.3-0.4 in Alcator C-Mod) similar to those of the alpha heating and ICRH/ECRH heating systems in ITER;
- Lack of central source of neutral particles, as additional heating is RF-based without neutral beam injection, similar to the situation with 1 MeV beams in ITER;
- Low toroidal rotation (typically $M_D \leq 0.05$ in these experiments, which is in the low range of toroidal rotation speeds in Alcator C-Mod) similar to that expected in ITER because of the low momentum input with the high energy beams, leading to poloidally symmetric high-Z impurity density.

Experiments were performed by injecting W by the laser blow-off technique (LBO) [36]. The key measurements of kinetic plasma parameters used for the studies presented in this paper are: Thomson scattering for the electron density and temperature, electron cyclotron emission for the electron temperature [37], X-ray imaging crystal spectrometry for ion temperature and toroidal rotation profile measurements [38]. For the characterization of W transport and plasma radiation evolution associated with the W LBO injection the key measurements are provided by: radially and vertically viewing Soft X-ray tomography by two 38-channel arrays [37] (equipped with a 50 μm Be filter), a horizontally viewing midplane AXUV (Absolute eXtreme Ultra-Violet) diode array and set of resistive bolometers [39] and a pair of radially viewing, flat-field VUV spectrometers (1-7 nm, 10-30 nm) [40].

An example of the typical evolution of the plasma parameters in these experiments is shown in Fig. 5 for two ICRH heating power levels. Although the intensity of the laser for W LBO was adjusted to keep the W injection to the minimum required for diagnostic purposes, the associated radiation increase and changes to the edge plasma following the W LBO were sufficient to trigger a back transition into L-mode in the low power (black in Fig. 4) case. This limited the lower range of ICRH power for which W transport could be characterized in H-mode by this technique for some of the conditions explored. At higher powers, as shown in Fig. 5, the effect of the W LBO was much less perturbing and the plasma remained in H-mode without major modifications of its parameters. The electron and ion temperature and electron density from the diagnostics above for the two example discharges in Fig. 5 are shown in Fig. 6. As can be seen in Fig. 6 and quantified in Table 2, the overall peaking of the core density and temperature profiles, characterized by the ratio of its values at normalized

radius ($\rho = r/a$) $\rho = 0$ and 0.7 are similar for ITER Q_{DT} =10 plasmas and for Alcator C-Mod. If anything, the Alcator C-Mod profiles for high P_{ICRH} levels are less favourable for W transport (more likely core W peaking) than those of ITER in terms of the relative ion temperature to density peaking. This is somewhat compensated by the fact that, due to the lower collisionality of W in ITER compared to Alcator C-Mod, the effective temperature screening factor for W is 0.35-0.4 in ITER instead of 0.5 Alcator C-Mod, where W is in the Pfirsch-Schlüter collisionality regime. This relatively low ion temperature profile peaking is due to the lower level of equipartition in Alcator C-Mod at these densities and to the dominant electron heating which leads to a large increase of the T_e/T_i ratio (from 1.4-1.8) as the ICRH power is increased. This is unlike ITER where equipartition is dominant and $T_e/T_i \sim 1$ despite the dominant electron heating. In general the relation between the ion temperature gradient and the density gradient in Alcator C-Mod is found to be favourable for W transport in the central region of the plasma ($\rho \leq 0.35$) if W were dominated by neoclassical transport in this region; while further out the situation is opposite, as shown in Fig. 7. Increasing the central ICRH heating power reduces the scale length of the ion temperature with respect to the density (thus making W neoclassical transport to be outwards in the central region) while further out the effect is opposite.

Regarding other impurity-related transport aspects, these discharges are indeed very comparable to ITER. The toroidal rotation velocity in the core plasma is typically low with $M_D \leq 0.1$ and, correspondingly, poloidally symmetric impurity profiles are measured for these discharges.

4. Observations on W dynamics and transport in ITER-like H-mode plasmas in Alcator C-Mod.

An example of the typical evolution of the AXUV and spectroscopic line emission following the W LBO in these experiments is shown in Fig. 8. As shown in this figure the propagation of the radiation increase associated with the propagation of W into the plasma in these experiments is very fast up to $\rho \sim 0.3$ (within 3 ms); from there inwards transport is much slower and the rise of the W associated emission takes place in timescales of 15 ms. This is confirmed by a similar prompt rise of W unresolved transition array (UTA) emission characteristic of $W^{27+-35+}$ and a much slower evolution of line emission from $W^{42+-44+}$. This temporal evolution of the W emission in the plasma within $\rho \leq 0.8$ for can be modelled with the STRAHL code [41] by assuming a radially variable diffusion coefficient for W transport (without any convective velocity) with a very low value within the $\rho \leq 0.3$ region ($D_W \sim 4\ 10^-$

^{2} m^2s^{-1}, which is similar to the expected value of the W neoclassical diffusion coefficient in this region). For $\rho > 0.3$ the value of D_W required to model the fast propagation of W is typically one to two orders of magnitude larger (0.3-3 m^2s^{-1}). These findings are in excellent agreement with expectations for ITER shown in Fig. 2.b. Indeed modelling of Alcator C-Mod plasmas with ASTRA, on the basis of the experimental power deposition profiles determined by TRANSP analysis and with the same assumptions that those utilized to model ITER, reproduces qualitatively the same main plasma parameter profiles and W transport behaviour seen in the experiment, as shown in Fig. 9. The plasma density and electron and ion temperature profiles predicted for Alcator C-Mod have similar magnitude and gradients to those measured, as shown in Fig. 9.a. Also W transport is indeed found to be neoclassical in the plasma centre with $D^{neo}_W \sim 10^{-2}$ m^2s^{-1}, while it is anomalous further out with typical $D^{anomalous}_W \sim 0.2\text{-}2.0$ m^2s^{-1}, as shown in Fig. 9.b. Both D_W values are similar to those deduced by STRAHL from the time evolution of the W emission following the LBO mentioned above. Quantitatively there are differences between experiment and the ASTRA modelling regarding the extent of the region with negligible anomalous W transport, which is $\rho \leq 0.15$ in the ASTRA simulations while it is $\rho \leq 0.3$ in experiment. This discrepancy and those in the predicted density and temperature profiles compared to the experimental profiles in Fig. 9 can be resolved by tuning input parameters in the GLF23 model, which will be the subject of a future publication.

In agreement with the ITER expectations and with the relation of the density and temperature scale lengths measured in these Alcator C-Mod plasmas (see Fig. 7.a), there is no evidence for strong, steady-state W peaking in the central region of the plasmas in these discharges, as shown in Fig. 10. In this figure the W density profile after penetration of the W injected by LBO to the plasma core is derived from the radiated power profiles from resistive bolometers and from soft X-ray tomography, averaging over multiple sawteeth. For both ways to evaluate the W profile, this is found to be rather flat in the plasma core and in all cases less peaked that the corresponding electron density profile in the same region. It is important to remark that there is no sign of W density peaking in the outer regions of the plasma ($0.35 \leq \rho \leq 0.55$) even for conditions in which neoclassical transport would predict it on the basis of the local plasma density and ion temperature scale lengths in Fig. 7.a. This is consistent with the fact that in that region W anomalous transport is dominant and that $D_W^{anomalous} \sim (10\text{-}100)\ D_W^{neo}$ so that the resulting W peaking is one to two orders of magnitude lower than evaluations made on the basis of neoclassical transport alone. Therefore, the

peaking of the main ion density caused by anomalous transport in these plasmas (and expected in ITER, which could increase its fusion performance for given edge MHD pressure limits) for $0.3 < \rho < 0.8$ does not bring associated with it any drawback regarding W density peaking in this region, consistent with the ITER modelling results in Fig.1.a and 2.a.

An interesting issue that has been possible to address in the Alcator C-Mod experiments, and which is difficult to address by modelling for ITER (as discussed in Sect. 2), is whether there is a significant W density peaking between sawteeth in these plasmas with ITER-like sawtooth-averaged peaked plasma density profiles. This has been assessed by analysing the increase of the soft X-ray emission between sawteeth compared to that expected from the change of radiation emission efficiency, $L_{W,SXR}$ (T_e), caused by the change of the electron temperature inside the sawtooth inversion radius between sawteeth. As shown in Fig. 11, the increased soft X-ray emissivity due to tungsten:

$$\delta\varepsilon_{SXR} = n_e n_W L_{W,SXR}(T_e) \qquad (4)$$

in the plasma central region inside the sawtooth inversion radius can increase by a factor of ~ 1.8 when the electron temperature increases by ~ 33 % from 3 to 4 keV. This increased peaking of the soft X-ray emission between sawteeth could in principle be due to an increase of the W density itself (i.e. there would be W accumulation between sawteeth and W expulsion from the core by sawteeth) or due to the increased peaking of the temperature. Analysis of the change to the W soft X-ray radiation due to the change of temperature has been carried out by using two sets of W emission modelling for $L_{W,SXR}$, following the procedures in [11] but accounting for the thinner Be filter. This reveals that most of the experimentally observed increase between sawteeth can be attributed to an increase by a factor of 1.4-1.5 of the soft X-ray radiation efficiency when the temperature increases from 3 to 4 keV. The residual increase up to the measured 1.8 could be compatible with an increase of the electron density by ~ 10% between sawteeth at constant W concentration.

In order to confirm in detail the conclusions extracted from the sawtooth-averaged W density profile in Fig. 10 and of its possible change between sawteeth in Fig. 11, detailed analysis of the radial scale length of the soft X-ray emission in the core region ($\rho = 0.15$) has been carried out in order to determine what the W density scale length compatible with these measurements is and what could be its variation along the sawtooth cycle. Expanding Eq. 4:

$$\frac{a}{L_\varepsilon} = \frac{a}{L_{n_e}} + \frac{a}{L_{n_W}} + \frac{T_e}{L_W}\frac{dL_W}{dT_e}\frac{a}{L_{T_e}} \qquad (5)$$

shows that the emissivity scale length, L_ε, can be used as a proxy for the tungsten density scale length, L_{nW}. From the experimental data for the measured electron density and

temperature scale lengths (see e.g. Fig. 7.b), their variations between sawteeth (a/L_{ne} nearly constant and a/L_{Te} increasing from 0 to its stiff, sawtooth-averaged value), the deduced values for $a/L\varepsilon$ assuming that $a/Ln_W = 0$ are shown in Table 3.

Calculation of the inverse scale length of the soft X-ray emission at $\rho = 0.15$ shown in Figure 11 indicates little variation between sawteeth (after the initial phase immediately after the flattening of the temperature by the sawtooth) and that a quasi-stationary level is reached during each sawtooth prior to the destabilization of the m/n=1/1 precursor mode. Fig. 12.a shows the trajectories of $a/L\varepsilon$ versus T_e within the sawtooth cycle for an ICRF power scan demonstrating that within the experimental variations of the electron density and temperature scale lengths and of the normalized radiation efficiency with temperature, there is no need to invoke strong W density peaking (i.e. a large a/Ln_W in Eq. 5) to explain the variation of $a/L\varepsilon$ in the sawtooth cycle. The range of the inverse scale lengths of the soft X-ray radiation emission in Fig. 12.a is similar to that from expectations in Table 3, which are evaluated on the basis of the assumption of flat W profiles with $a/Ln_W = 0$. From the upper values of the inverse scale lengths of the soft X-ray radiation emission in Fig. 12.a, a value of $a/Ln_W \sim 1$-2 could be compatible with these experimental measurements. It should be noted that this value of the W density scale length is in good agreement with that from neoclassical transport of W in Alcator C-Mod evaluated with the measured plasma density and ion temperature profiles; i.e. $a/Ln_{Wneo} = aV_W^{neo}/D_W^{neo} = 1 - 2$.

Deviations from this picture have been identified in cases where there is off-normal MHD activity (not discussed in this paper) and when the H minority density has been increased from the usual the 3-4% to a much higher level of 10%. This is shown in Fig. 12.b, where strong peaking of the soft X-ray radiation emission is found between sawteeth which is well above the range of values in Table 3 and indicate that strong W peaking takes place in these conditions. When the hydrogen level is increased by main-chamber H_2 puffing at fixed power, $a/L\varepsilon$ increases by a factor of 3, while increasing the ICRF power at $H/(H+D) \sim 0.1$ reduces the emissivity peaking. This is believed to be due to the influence of friction between the high energy minority ions and the W ions, which is well described by neoclassical transport along the initial modelling studies in [12]. This will be the subject of further modelling and experimental studies in Alcator C-Mod.

5. Summary, Conclusions and further R&D.

The results obtained in the Alcator C-Mod experiments described in this paper have provided for the first time an experimental characterization of the behaviour of W in H-mode

plasmas with several ITER-like characteristics including: plasma density peaking, low/no central source of neutral, electron dominant heating (with $T_e/T_i < 2$) and low core plasma toroidal rotation ($M_D < 0.1$).

The major result obtained in these experiments is that under such conditions no strong core W peaking is typically obtained. Exceptions are cases with strong MHD activity or when very high H minority concentrations are used for ICRH heating. This experimental result can be explained by W transport being dominated by anomalous W transport with a large diffusive component across the plasma cross section in the range $0.3 < \rho < \rho_{ETB}$ (where ETB is the inner point of the edge transport barrier), while inside $\rho < 0.3$ W transport is better described by neoclassical transport, which is in good agreement with finding in other experiments [11]. On the other hand and contrary to these other experiments, the scale lengths for the plasma temperature and density inside $\rho < 0.3$ are such that core neoclassical transport of W does not have a strong inward pinch and, thus, W does not accumulate in the plasma core. Here the fact that these plasmas are ITER-like in terms of the core source of neutrals (i.e. no/very low source of neutrals provided by the NBI+RF heating systems) is key to prevent the excessive core density peaking found in NBI dominated experiments that show strong W accumulation [11].

In addition, the timescales for W diffusion inwards from the anomalous transport dominated zone into the central plasma region ($a_p \leq 0.3$ a) where anomalous transport is negligible are well described by neoclassical transport expectations for the Alcator C-Mod plasmas with very low plasma rotation. This provides a solid basis for the extrapolation of this timescale to ITER. The W transport timescales found in Alcator C-Mod can be extrapolated to ITER by taking into account that:

$$\frac{\tau_W^{ITER}}{\tau_W^{C-Mod}} = \frac{a_{p-ITER}^2}{a_{p-C-Mod}^2} \frac{D_{C-Mod}^{neoc.}}{D_{ITER}^{neoc.}} \quad (6)$$

which corresponds to $\tau_W{}^{ITER} = 3.5$ s for $\tau_W{}^{C\text{-}Mod} = 15$ ms, assuming that the ratio a_p/a is similar in Alcator C-Mod and ITER, which is well justified on the basis of the ITER modelling results in Fig. 2 and Alcator C-Mod experimental observations in Fig. 8. From this large ratio between ITER and Alcator C-Mod a factor of ~ 80 comes from the device size and the remaining factor of 3 from the difference in neoclassical transport diffusion coefficients between the two devices (note that the magnetic field in these Alcator C-Mod discharges is virtually the same of ITER $Q_{DT} = 10$ plasmas). This shows that W accumulation in ITER, if it were to occur, can be detected well in advance of when it may cause excessive W radiation and affect plasma performance. A timescale of 3.5 s allows core heating to be applied to arrest

such possible W peaking well in advance of the point when it has a detrimental effect on plasma performance, as shown in the ITER modelling results of Sect. 2. Last but not least, these Alcator C-Mod experiments results show that, although sawtooth modulate the W density in the central plasma region, this effect is not required to explain the lack of W peaking in the experiments. This implies that the lack of sawtooth-averaged W density peaking in these ITER-like H-mode plasmas in Alcator C-Mod is not driven by the repetitive flattening of the W density profile by the sawteeth but by the fact that inter-sawtooth central W transport does not lead to strong central W density peaking, in agreement with similar recent observations at JET [15, 42], which is a key result for ITER.

The efficiency of sawteeth to expel W from the core plasma is determined by the ratio of the time that it takes W to diffuse/convect into the core plasma (τ_W^{core}) to the sawtooth repetition period ($\tau_{sawtooth}$). In the Alcator C-Mod discharges studied, the typical value of τ_W^{core} is ~ 10 ms, as discussed above, while the typical sawtooth period is $\tau_{sawtooth}$ ~10 ms (see Fig. 11 for an example). In these circumstances the effectiveness of sawteeth to expel W from the core is potentially very high, as $\tau_W^{core}/\tau_{sawtooth}|_{C\text{-}Mod} \sim 1$. This means that, even if W would strongly peak in the core plasma between sawteeth in Alcator C-Mod, the sawtooth averaged W density peaking would be much lower (typically ~ ½ of the peaking before sawteeth). On the contrary, for ITER the expected sawtooth period for Q_{DT} =10 plasmas is expected to be very long $\tau_{sawtooth}$ ~30-40 s [43], due to stabilizing effects of fast particles (produced by the additional heating systems and the alpha particles themselves) on the MHD sawtooth trigger. This should be compared with the typical τ_W^{core} ~ 3.5 s leading to $\tau_W^{core}/\tau_{sawtooth}|_{ITER} \sim 0.1$. In ITER, therefore, the effectiveness of sawteeth to expel W from the core is expected to negligible and intra-sawtooth transport dominates the core peaking of W. In this respect, it is an important experimental finding that for these ITER-like H-mode plasmas in Alcator C-Mod it is the intra-sawtooth transport which leads to flat core W profiles and that these flat profiles are not the consequence of sawtooth activity, as the latter would be very ineffective in ITER.

Overall, the Alcator C-Mod experiments show that the key modelling assumptions and modelling results obtained for ITER in Sect. 2 are well based on the experimental results from ITER-like H-mode plasmas in Alcator C-Mod. Thus the positive picture regarding the lack of strong W peaking in ITER reference Q_{DT}=10 plasmas is well justified on present understanding. In this respect, the fact that the ITER NBI heating system provides a source of particles in the core plasma with a density rate two to three orders of magnitude lower than in

present NBI-dominated experiments is key for this positive picture regarding core W transport in ITER; which is well justified by the RF heated Alcator C-Mod experimental results presented here. In addition, ITER modelling and the Alcator C-Mod experiments show that the expected density peaking from anomalous transport in the region $0.3 < \rho < \rho_{ETB}$, which can be beneficial to improve fusion performance in ITER, does not have a negative impact regarding W peaking in the $0.3 < \rho < \rho_{ETB}$ region because W transport in that region is dominated by diffusive anomalous transport with a large diffusion coefficient in the modelled ITER plasmas. This is in excellent agreement with the observations of W penetration (following W LBOs) into the core plasma of the Alcator C-Mod ITER-like H-modes with ITER-like density peaking and thus a robust prediction for ITER.

While the results obtained in these Alcator C-Mod experiments are very encouraging regarding the expected features of core W transport in ITER, there remain open questions regarding the latter and also on the extrapolability of the results of the Alcator C-Mod experiments to ITER. One such question concerns the role of fast particles on neoclassical W transport in Alcator C-Mod and expectations for ITER. Fast particle species and energy distributions will be very different in ITER (alpha particles with ~3.5 MeV energies, 1 MeV fast D ions from NBI, fast T, H or He^3 from ICRH heating,…) from those in Alcator C-Mod (H-minority accelerated ions). Present understanding shows that fast ions can influence W density peaking in the central plasma due to friction between high energy ICRH minority ions and W ions [12]. This could change the W density profiles in the central plasma region in ITER with respect to the modelling based on the thermal plasma parameters alone shown in Sect. 2. Initial results from Alcator C-Mod ITER-like H-mode experiments indicate that W peaking could be higher than what is expected from the thermal plasma parameters for some fast particle distributions, such as those obtained with high percentage of hydrogen minority. Another open question concerns the lower equipartition and higher T_e/T_i ratio found in Alcator C-Mod with respect to ITER, given the different degrees of stiffness of the electron and ion temperature profiles and the different effects of pushing these two temperature profiles against their stiff limits on the density profiles seen in Alcator C-Mod experiments and in ITER modelling. Further experiments and modelling of the existing experimental results presented here are required to make progress in these two areas. This could include additional experiments in Alcator C-Mod by varying the minority concentration level, ICRH resonance location, electron to ion heating ratio by using He^3 minority as foreseen for ITER, etc.

Finally, another area where more analysis, experiments and modelling are required is the one regarding the characterization of the processes leading to the expulsion of W outside the ETB in ITER-like H-mode plasmas, which has not been discussed in this paper. In conditions in which no strong W peaking takes place this is regulated by the exhaust of W through the ETB, which for the Alcator C-Mod plasmas studies here is related to the edge turbulent transport associated with the EDA regime (and with the effective transport by controlled ELMs in ITER) and with the underlying neoclassical transport in the ETB region. The results obtained in these Alcator C-Mod experiments show that the typical W confinement time in the plasma (i.e. the typical timescale for the central W emission to decay after the LBO) can vary from ~ 50 to 200 ms when the LBO does not trigger an H-L transition, as shown in Fig. 13. It remains to be understood whether changes of edge turbulent transport or of the neoclassical transport in the ETB with the variation of plasma parameters explored dominate the observed changes on the W confinement time and how these physics processes extrapolate to ITER.

Acknowledgements

The authors would like to thank the Alcator C-Mod operations staff, particularly S. Wolfe, for their contribution to the success of the experiments reported in this paper, C. Angioni and P. Mantica for helpful discussions on the ITER W modelling, E. Belli and J. Candy for their support on the NEO modelling and M. O'Mullane for providing atomic data required for the interpretation of the soft-X ray signals. This work was supported by the US Department of Energy Agreement DE-FC02-99ER54512.

Disclaimer

The views and opinions expressed herein do not necessarily reflect those of the ITER Organization.

6. References.

[1] D. J. Campbell for the ITER Organization, Domestic Agencies and ITER collaborators, in Fusion Energy 2012 (Proc. 24th Int. Conf. San Diego), Paper ITR/P1-18.

[2] A. Kallenbach, R. Neu, R. Dux, H.-U. Fahrbach, J. C. Fuchs, L. Giannone, O. Gruber, A. Herrmann, P.T. Lang, B. Lipschultz, C.F. Maggi, J. Neuhauser, V. Philipps, T. Pütterich, V. Rohde, J. Roth, G. Sergienko, A. Sips and ASDEX Upgrade Team, Plasma Phys. Control. Fusion **47** (2005) B207.

[3] P. C. de Vries, G. Arnoux, A. Huber, J. Flanagan, M. Lehnen, V. Riccardo, C. Reux, S. Jachmich, C. Lowry, G. Calabro, D. Frigione, M. Tsalas, N. Hartmann, S. Brezinsek, M. Clever, D. Douai, M. Groth, T. C. Hender, E. Hodille, E. Joffrin, U. Kruezi, G. F. Matthews,

J. Morris, R. Neu, V. Philipps, G. Sergienko, M. Sertoli and JET EFDA contributors, Plasma Phys. Control. Fusion **54** (2012) 124032.

[4] T. Pütterich, R. Dux, M.A. Janzer, R.M. McDermott and the ASDEX Upgrade Team, J. Nucl. Mat. **415** (2011) S334.

[5] T. Sunn Pedersen, R.S. Granetz, A.E. Hubbard, I.H. Hutchinson, E.S. Marmar, J.E. Rice and J. Terry, Nucl. Fusion **40** (2000) 1795.

[6] M. Greenwald, R. Boivin, P. Bonoli, R. Budny, C. Fiore, J. Goetz, R. Granetz, A. Hubbard, I. Hutchinson, J. Irby, B. LaBombard, Y. Lin, B. Lipschultz, E. Marmar, A. Mazurenko, D. Mossessian, T. Sunn Pedersen, C. S. Pitcher, M. Porkolab, J. Rice, W. Rowan, J. Snipes, G. Schilling, Y. Takase, J. Terry, S. Wolfe, J. Weaver, B. Welch, and S. Wukitch, Phys. Plasmas **6** (1999) 1943.

[7] T.E. Evans, R.A. Moyer, K.H. Burrell, M.E. Fenstermacher, I. Joseph, A.W. Leonard, T.H. Osborne, G.D. Porter, M.J. Schaffer, P.B. Snyder, P.R. Thomas, J.G. Watkins and W.P. West, Nature Physics **2** (2006) 419.

[8] A. Loarte, G. Huijsmans, S. Futatani, L.R. Baylor, T.E. Evans, D. M. Orlov, O. Schmitz, M. Becoulet, P. Cahyna, Y. Gribov, A. Kavin, A. Sashala Naik, D.J. Campbell, T. Casper, E. Daly, H. Frerichs, A. Kischner, R. Laengner, S. Lisgo, R.A. Pitts, G. Saibene and A. Wingen, Nucl. Fusion **54** (2014) 033007.

[9] R. Neu, R. Dux, A. Geier, A. Kallenbach, R. Pugno, V. Rohde, D. Bolshukhin, J.C. Fuchs, O. Gehre, O. Gruber, J. Hobirk, M. Kaufmann, K. Krieger, M. Laux, C. Maggi, H. Murmann, J. Neuhauser, F. Ryter, A.C.C. Sips, A. Stäbler, J. Stober, W. Suttrop, H. Zohm and the ASDEX Upgrade Team, Plasma Phys. Control. Fusion **44** (2002) 811.

[10] T. Pütterich, R. Dux, R. Neu, M. Bernert, M.N.A. Beurskens, V. Bobkov, S. Brezinsek, C. Challis, J.W. Coenen, I. Coffey, A. Czarnecka, C. Giroud, P. Jacquet, E. Joffrin, A. Kallenbach, M. Lehnen, E. Lerche, E. de la Luna, S. Marsen, G. Matthews, M.-L. Mayoral, R.M. McDermott, A. Meigs, J. Mlynar, M. Sertoli, G. van Rooij, the ASDEX Upgrade Team and JET EFDA Contributors, Plasma Phys. Control. Fusion **55** (2013) 124036

[11] C. Angioni, P. Mantica, T. Pütterich, M. Valisa, M. Baruzzo, E.A. Belli, P. Belo, F.J. Casson, C. Challis, P. Drewelow, C. Giroud, N. Hawkes, T.C. Hender, J. Hobirk, T. Koskela, L. Lauro Taroni, C.F. Maggi, J. Mlynar, T. Odstrcil, M.L. Reinke, M. Romanelli and JET EFDA Contributors, Nucl. Fusion **54** (2014) 1083028.

[12] F.J. Casson, C. Angioni, E.A. Belli, R. Bilato, P. Mantica, T. Odstrcil, T. Puetterich, M. Valisa, L. Garzotti, C. Giroud, J. Hobirk, C.F. Maggi, J. Mlynar, M.L. Reinke, JET EFDA contributors and the ASDEX-Upgrade team, 41st European Physical Society Conference on Plasma Physics, Berlin, Germany, 2014, to be published in Plasma Phys. Control. Fusion. (http://arxiv.org/abs/1407.1191).

[13] R. Dux, A.G. Peeters, A. Gude, A. Kallenbach, R. Neu and ASDEX Upgrade Team, Nucl. Fusion **39** (1999) 11.

[14] P. Mantica, C. Angioni, F.J. Casson, T. Pütterich, M. Valisa, M. Baruzzo, P.C. da Silva Aresta Belo, I. Coffey, P. Drewelow, C. Giroud, N.C. Hawkes, T.C. Hender, T. Koskela, L. Lauro Taroni, E. Lerche, C.F. Maggi, J.Mlynar, M. O'Mullane, M.E. Puiatti, M.L. Reinke, M. Romanelli and JET EFDA contributors, 41st European Physical Society Conference on Plasma Physics, Berlin, Germany, 2014, paper P1.017.

[15] M. Goniche, E. Lerche, P. Jacquet, D. Van Eester, V. Bobkov, S. Brezinsek, L. Colas, A. Czarnecka, P. Drewelow, R. Dumont, N. Fedorczak, C. Giroud, M. Graham, J.P. Graves, I.

Monakhov, P. Monier-Garbet, C. Noble, T. Pütterich, F.Rimini, M. Valisa and JET EFDA contributors, 41st European Physical Society Conference on Plasma Physics, Berlin, Germany, 2014, paper O4.129.

[16] C. Angioni and P. Helander, Plasma Phys. Control. Fusion **56** (2014) 124001.

[17] G. V. Pereverzev and P. N. Yushmanov, ASTRA - Automated System for Transport Analysis, Report IPP 5/98.

[18] R.E. Waltz, G.M. Staebler, W. Dorland, G.W. Hammett, M. Kotschenreuther and J.A. Konings, Phys. Plasmas **4** (1997) 2482.

[19] W. A. Houlberg, K. C. Shaing, S. P. Hirshman and M. C. Zarnstorff, Phys. Plasmas **4** (1997) 3230.

[20] V.M. Leonov and V.E. Zhogolev, Plasma Phys. Control. Fusion **47** (2005) 903.

[21] P.B. Snyder, R.J. Groebner, J.W. Hughes, T.H. Osborne, M. Beurskens, A.W. Leonard, H.R. Wilson and X.Q. Xu, Nucl. Fusion **51** (2011) 103016.

[22] C. Angioni, H. Weisen, O.J.W.F. Kardaun, M. Maslov, A. Zabolotsky, C. Fuchs, L. Garzotti, C. Giroud, B. Kurzan, P. Mantica, A.G. Peeters, J. Stober and the ASDEX Upgrade Team and contributors to the EFDA-JET Workprogramme, Nucl. Fusion **47** (2007) 1326.

[23] ITER Physics Expert Group on Confinement and Transport, ITER Physics Expert Group on Confinement Modelling and Database and ITER Physics Basis Editors, Nucl. Fusion **39** (1999) 2175.

[24] V. Parail, R. Albanese, R. Ambrosino, J.-F. Artaud, K. Besseghir, M. Cavinato, G. Corrigan, J. Garcia, L. Garzotti, Y. Gribov, F. Imbeaux, F. Koechl, C.V. Labate, J. Lister, X. Litaudon, A. Loarte, P. Maget, M. Mattei, D. McDonald, E. Nardon, G. Saibene, R. Sartori and J. Urban, Nucl. Fusion **53** (2013) 113002.

[25] R. Dux, R. Neu, A. G. Peeters, G. Pereverzev, A. Mück, F. Ryter, J. Stober and ASDEX Upgrade Team, Plasma Phys. Control. Fusion **45** (2003) 1815.

[26] R. Dux, IPP Report, IPP 10/27, 2004.

[27] E. A. Belli and J. Candy, Plasma Phys. Control. Fusion **50** (2008) 095010.

[28] I. H. Hutchinson, R. Boivin, F. Bombarda, P. Bonoli, S. Fairfax, C. Fiore, J. Goetz, S. Golovato, R. Granetz, M. Greenwald, S. Horne, A. Hubbard, J. Irby, B. LaBombard, B. Lipschultz, E. Marmar, G. McCracken, M. Porkolab, J. Rice, J. Snipes, Y. Takase, J. Terry, S. Wolfe, C. Christensen, D. Garnier, M. Graf, T. Hsu, T. Luke, M. May, A. Niemczewski, G. Tinios, J. Schachter and J. Urbahn, Phys. Plasmas **1** (1994) 1511.

[29] E. S. Marmar and Alcator C-Mod Group, Fusion Sci. Technol. **51** (2007) 261.

[30] J. E. Rice, J. L. Terry, J. A. Goetz, Y. Wang, E. S. Marmar, M. Greenwald, I. Hutchinson, Y. Takase, S. Wolfe, H. Ohikawa and A. Hubbard, Phys. Plasmas **4** (1997) 1605.

[31] J. E. Rice, J. A. Goetz, R. S. Granetz, M. J. Greenwald, A. E. Hubbard, I. H. Hutchinson, E. S. Marmar, D. Mossessian, T. Sunn Pedersen, J. A. Snipes, J. L. Terry and S. M. Wolfe, Phys. Plasmas **7** (2000) 1825.

[32] J. E. Rice, J. L. Terry, E. S. Marmar, R. S. Granetz, M. J. Greenwald, A. E. Hubbard, J. H. Irby, S. M. Wolfe and T. Sunn Pedersen, Fusion Sci. Technol. **51** (2007) 357.

[33] J.W. Hughes, B. LaBombard, J. Terry, A. Hubbard and B. Lipschultz, Nucl. Fusion **47** (2007) 1057.

[34] G. Federici, A. Loarte and G. Strohmayer, Plasma Phys. Control. Fusion (2003) **45** 1523.

[35] M. Greenwald, C. Angioni, J.W. Hughes, J. Terry and H. Weisen, Nucl. Fusion **47** (2007) L26.

[36] N. T. Howard, M. Greenwald and J. E. Rice, Rev. Sci. Instrum. **82** (2011) 033512

[37] N. P. Basse, A. Dominguez, E. M. Edlund, C. L. Fiore, R. S. Granetz, A. E. Hubbard, J. W. Hughes, I. H. Hutchinson, J. H. Irby, B. LaBombard, L. Lin, Y. Lin, B. Lipschultz, J. E. Liptac, E. S. Marmar, D. A. Mossessian, R. R. Parker, M. Porkolab, J. E. Rice, J. A. Snipes, V. Tang, J. L. Terry, S. M. Wolfe, S. J. Wukitch, K. Zhurovich, R. V. Bravenec, P. E. Phillips, W. L. Rowan, G. J. Kramer, G. Schilling, S. D. Scott and S. J. Zweben, Fusion Sci. Technol. **51**(2007) 476.

[38] M.L. Reinke, Y.A. Podpaly, M. Bitter, I.H. Hutchinson, J.E. Rice, L. Delgado-Aparicio, C. Gao, M. Greenwald, K. Hill, N.T. Howard, A. Hubbard, J.W. Hughes, N. Pablant, A.E. White and S.M. Wolfe, Rev. Sci. Instrum. **83** (2012) 113501.

[39] M.L. Reinke and I.H. Hutchinson, Rev. Sci. Instrum. **79** (2008) 10F306.

[40] M.L. Reinke, P. Beiersdorfer, N.T. Howard, E.W. Magee, Y. Podplay, J.E. Rice and J.L. Terry, Rev. Sci. Instrum. **81** (2010) 10D736.

[41] R. Dux, IPP Report, IPP 10/30, 2006

[42] J. P. Graves, M. Lennholm, I. T. Chapman, E. Lerche, M. Reich, V. Bobkov, R. Dumont, D. Van Eester, J. Faustin, M. Goniche, P. Jacquet, T. Johnson, Y. Liu, T. Nicolas, S. Tholerus, T. Blackman, I. S. Carvalho, R. Felton, V. Kiptily, I. Monakhov, M. F. F. Nave, C. Sozzi, M. Tsalas and JET EFDA Contributors, 41st European Physical Society Conference on Plasma Physics, Berlin, Germany, 2014, paper I5.120.

[43] T.C. Hender, J.C Wesley, J. Bialek, A. Bondeson, A.H. Boozer, R.J. Buttery, A. Garofalo, T.P Goodman, R.S. Granetz, Y. Gribov, O. Gruber, M. Gryaznevich, G. Giruzzi, S. Günter, N. Hayashi, P. Helander, C.C. Hegna, D.F. Howell, D.A. Humphreys, G.T.A. Huysmans, A.W. Hyatt, A. Isayama, S.C. Jardin, Y. Kawano, A. Kellman, C. Kessel, H.R. Koslowski, R.J. La Haye, E. Lazzaro, Y.Q. Liu, V. Lukash, J. Manickam, S. Medvedev, V. Mertens, S.V. Mirnov, Y. Nakamura, G. Navratil, M. Okabayashi, T. Ozeki, R. Paccagnella, G. Pautasso, F. Porcelli, V.D. Pustovitov, V. Riccardo, M. Sato, O. Sauter, M.J. Schaffer, M. Shimada, P. Sonato, E.J. Strait, M. Sugihara, M. Takechi, A.D. Turnbull, E. Westerhof, D.G. Whyte, R. Yoshino, H. Zohm and the ITPA MHD, Disruption and Magnetic Control Topical Group, Nucl. Fusion **47** (2007) S128.

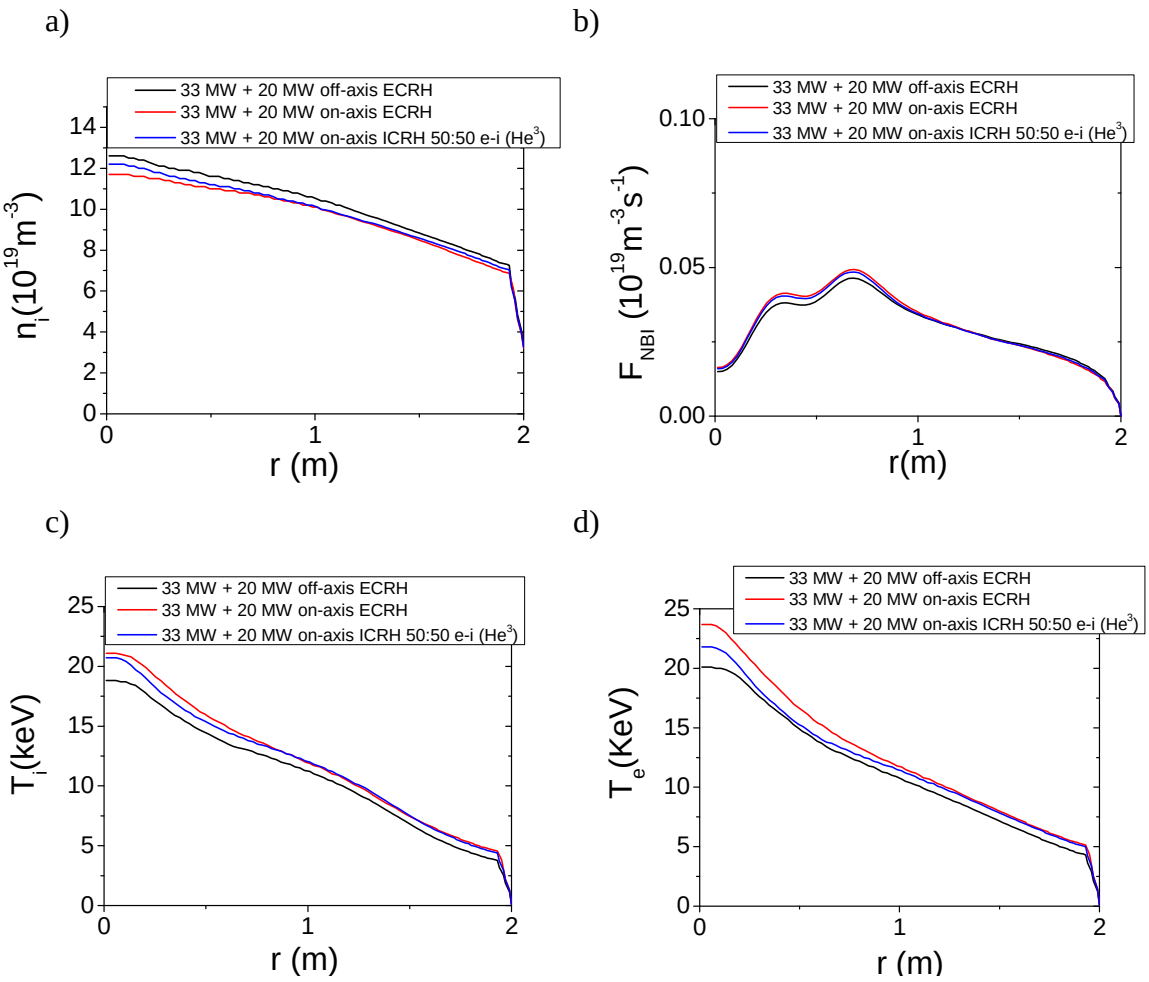

Figure 1. Results of ASTRA simulations for ITER 15 MA/5.3 T Q_{DT}=10 plasma with different heating schemes (33 MW of NBI + 20 MW of off axis or on axis ECRH and 33 MW of NBI + 20 MW of on axis ICRH with He^3 minority to provide maximum ion heating): a) ion density profile versus minor radius, b) NBI neutral source versus minor radius, c) ion temperature profiles versus minor radius and d) electron temperature profile versus minor radius.

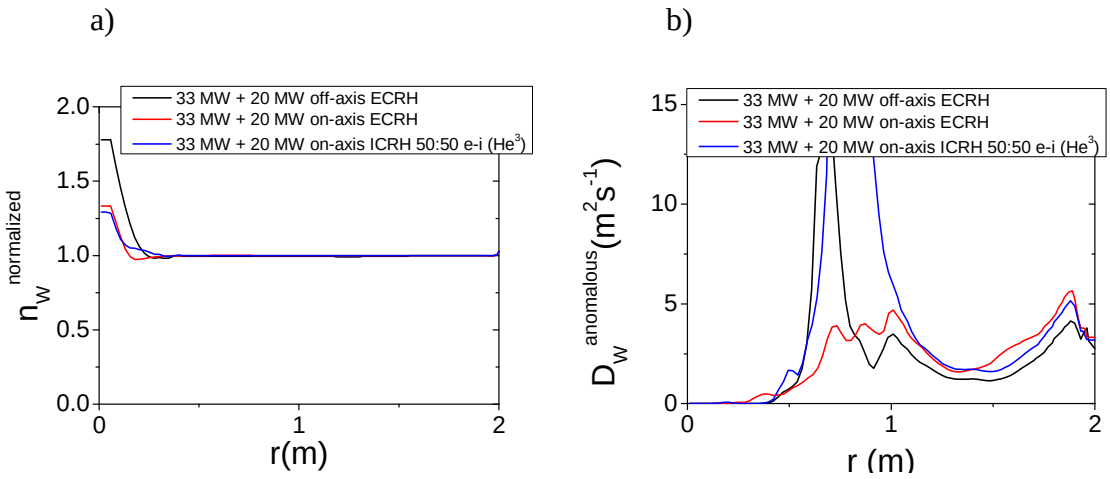

Figure 2. Results of ASTRA simulations for ITER 15 MA/5.3 T Q_{DT}=10 plasma with different heating schemes (33 MW of NBI + 20 MW of off axis or on axis ECRH and 33 MW of NBI + 20 MW of on axis ICRH with He^3 minority to provide maximum ion heating): a) normalized W density profile versus minor radius, b) anomalous diffusion coefficient for W transport as evaluated by the GLF23 transport model versus minor radius.

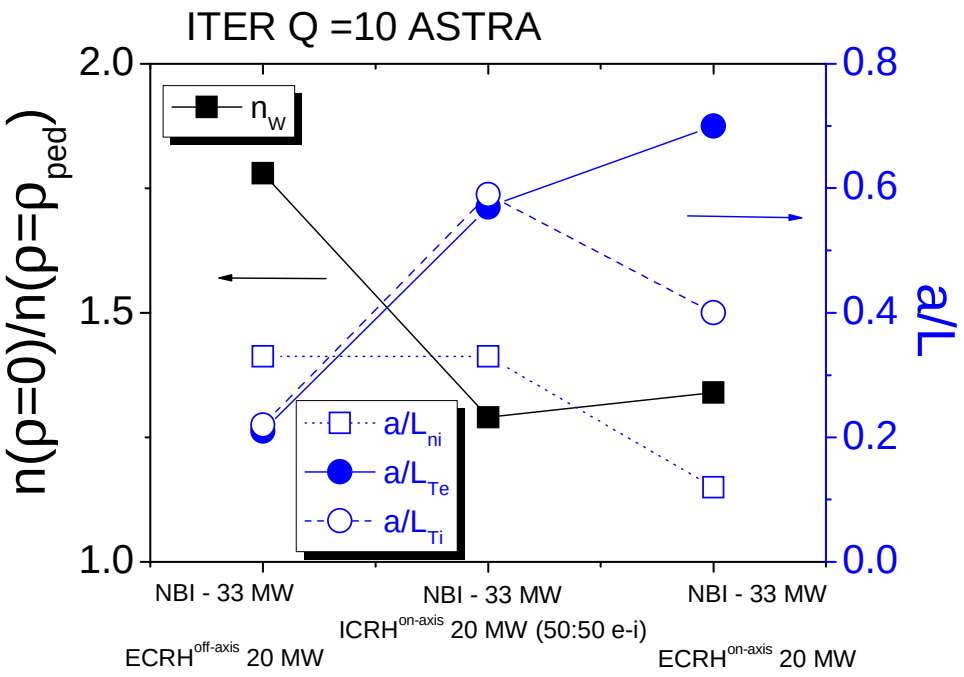

Figure 3. Results of ASTRA simulations for ITER 15 MA/5.3 T Q_{DT}=10 plasma with different heating schemes (33 MW of NBI + 20 MW of off axis or on axis ECRH and 33 MW of NBI + 20 MW of on axis ICRH with He^3 minority to provide maximum ion heating): Left axis) central W density peaking, Right axis) inversed normalized (to the minor radius) scale lengths for the ion density and ion and electron temperatures at r ~ 0.3 m.

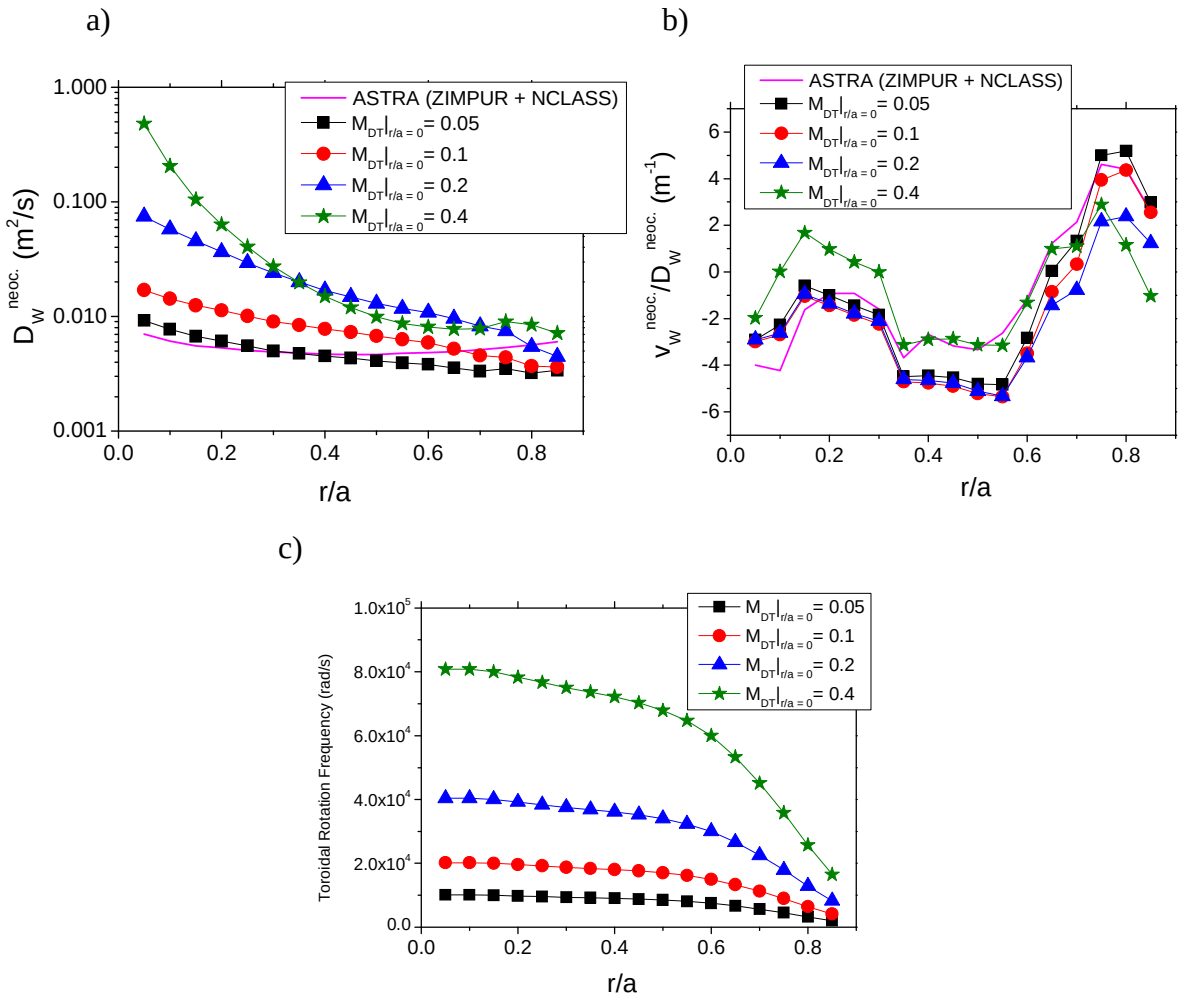

Figure 4. a) and b) Neoclassical transport coefficients (D_W and v_W/D_W) modelled with ZIMPUR+NCLASS (including all ionization stages of W) and with the NEO code for W^{63+}, for ITER plasma conditions with off-axis ECRH heating in Figs. 1 and 2 and a range of toroidal rotation velocities, showing the strong dependency of D_W and the weak dependency of v_W/D_W on the velocity of rotation except for its largest values. c) Rotation profiles used in the calculations in a) and b) obtained from re-scaling the ASTRA results to Mach numbers at r/a = 0 in the range of 0.05 0.4.

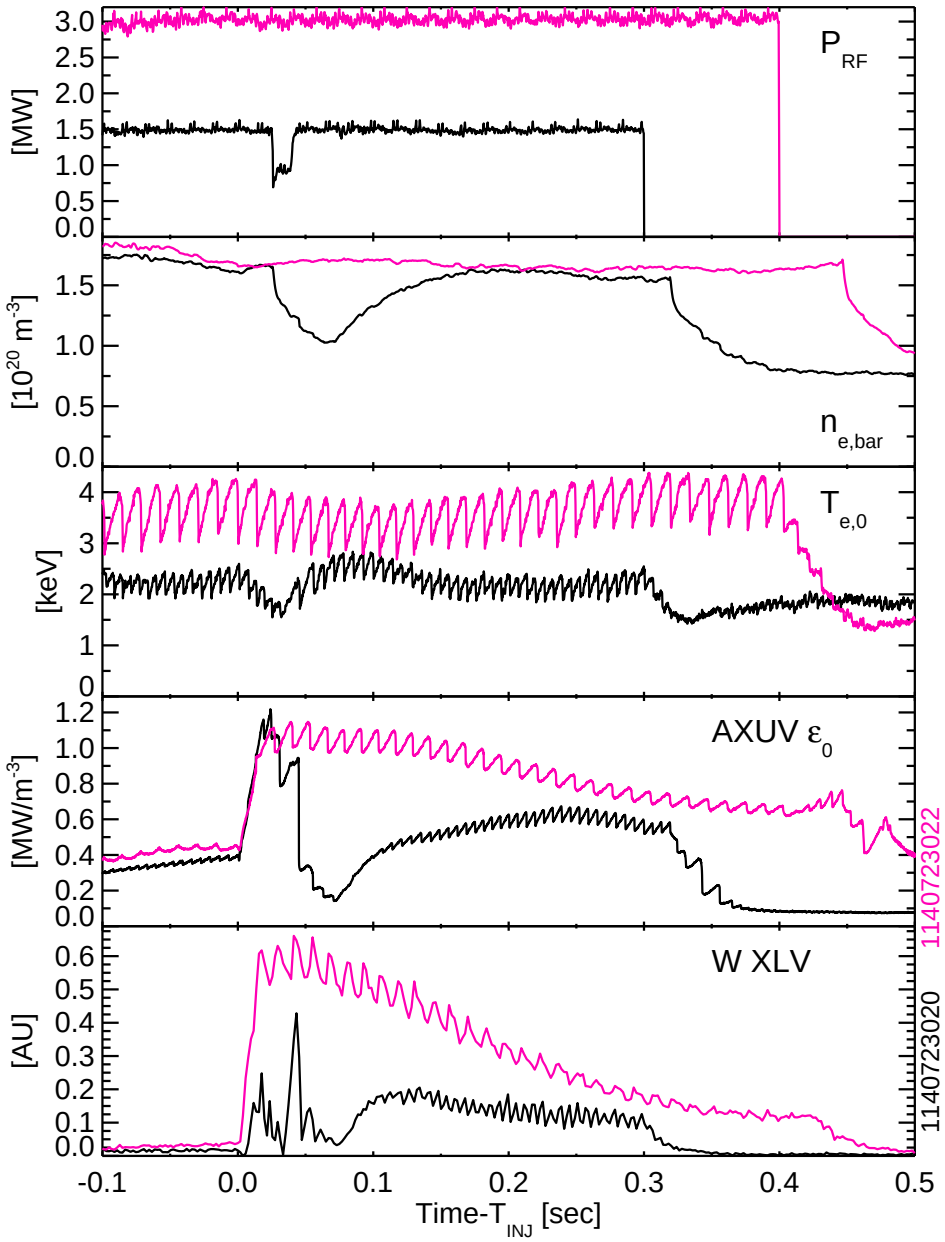

Figure 5. Measurements of plasma parameters and W emission in two typical Alcator C-Mod discharges with W LBO with I_p = 0.52 MA. From top to bottom: coupled ICRH power, line average density measured by the interferometer, central electron temperature measured by ECE, central extreme ultraviolet emission, and line-integrated emission from W^{44+}, a near-core charge state.

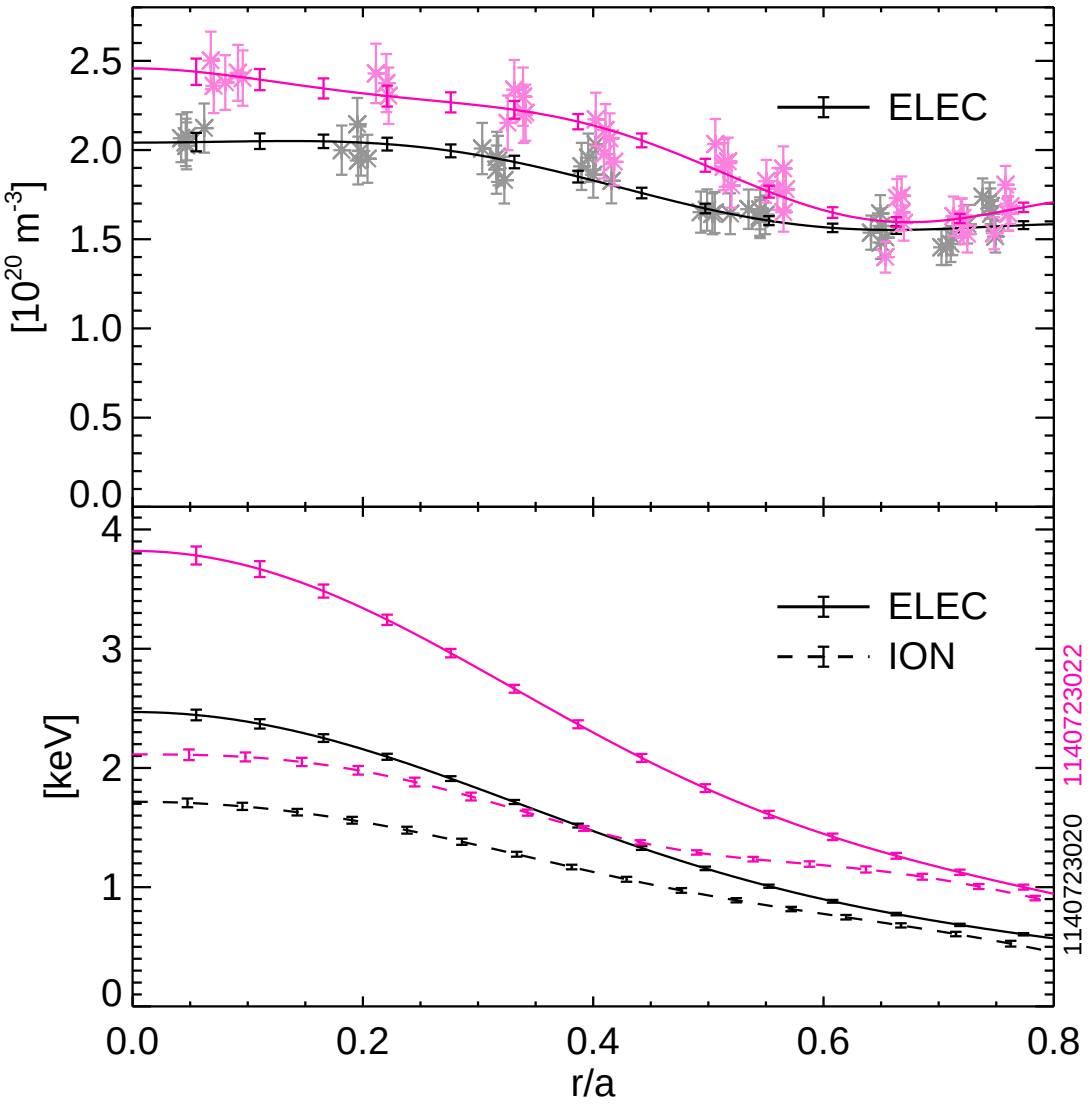

Figure 6. Measurements of electron plasma density (top) and electron and ion temperatures (bottom) for the discharges in Fig. 5 (black P_{ICRH} = 1.5 MW and magenta P_{ICRH} = 3.0 MW).

a) b)

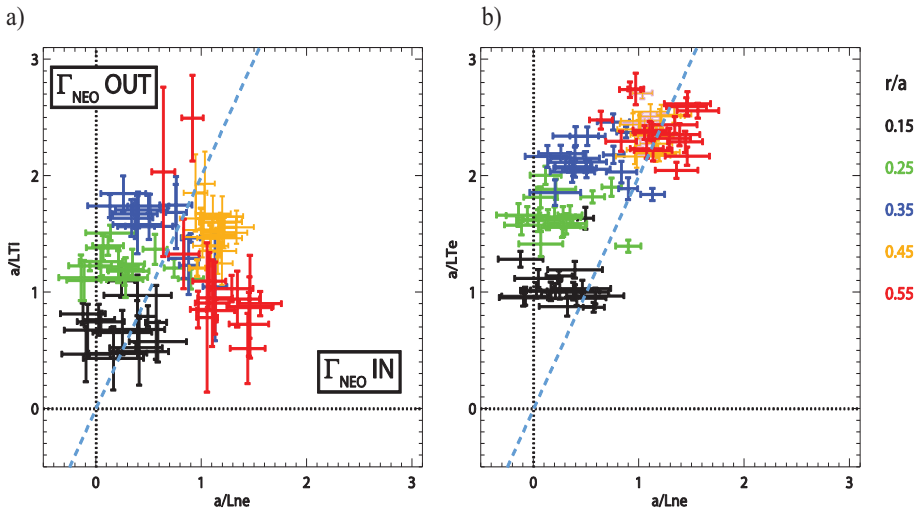

Figure 7. Measurements of the ion (a) and electron temperature (b) normalized inverse scale lengths versus electron density inverse scale lengths for a set of C-Mod discharges at various radial locations across the plasma core within $0.15 \leq \rho \leq 0.55$. The line for which $a/L_{Ti,e} = a/(2L_{ne})$ determining (when ion parameters are considered) the direction of neoclassical transport for W according to Eq. 1 is shown for reference.

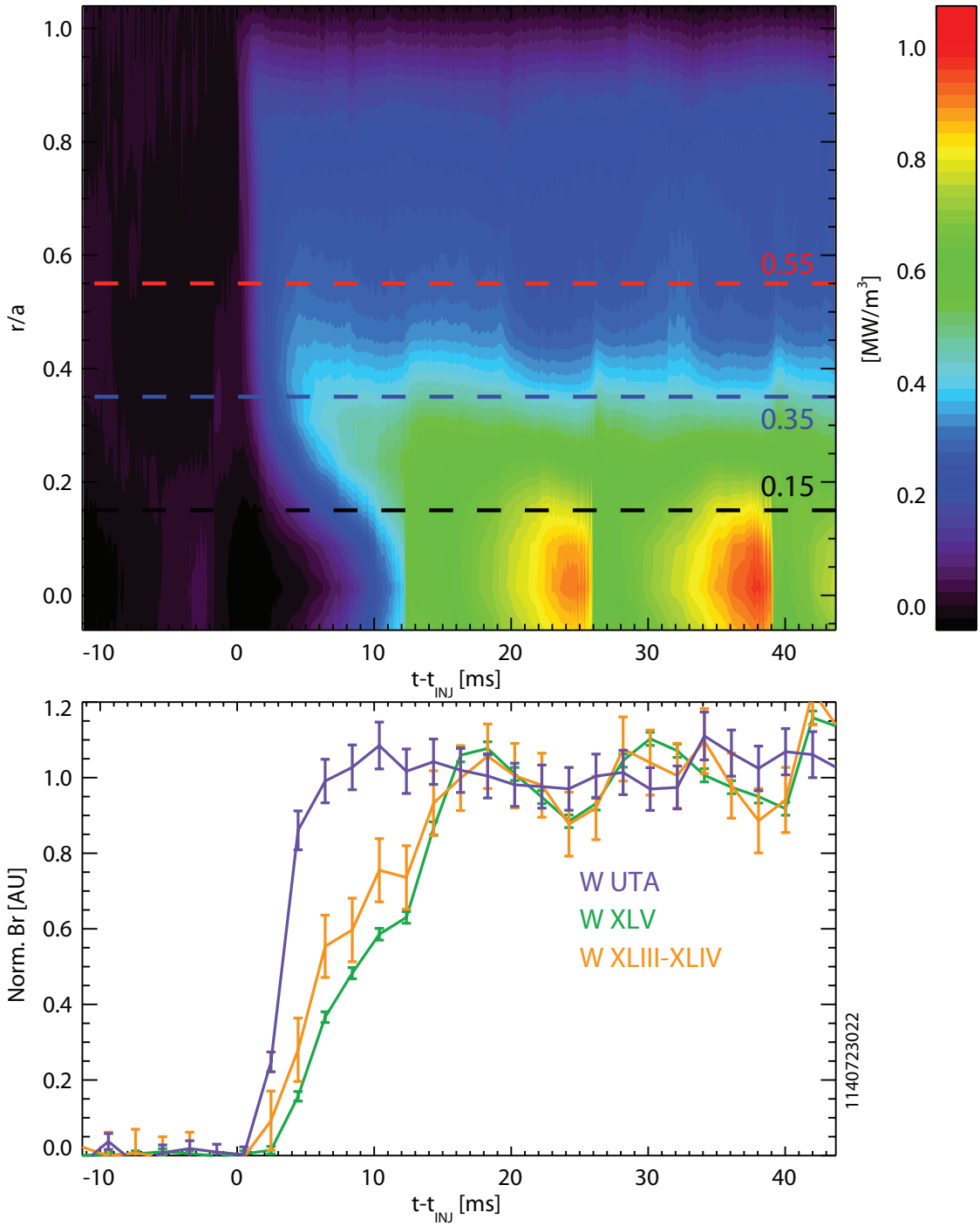

Figure 8. Measured time evolution of the AXUV diode emission (top) and spectroscopic line emission (bottom) following W injection by LBO (t = 0 ms is the LBO time) in an ITER-like Alcator C-Mod H-mode plasma. A fast inward propagation of the W emission up to $\rho = 0.3$ takes place within few ms; further penetration to $\rho = 0.0$ requires typically 10 ms or more. The modulation of the W emission signal after t = 20 ms for $\rho \leq 0.4$ is due to sawteeth.

a) b)

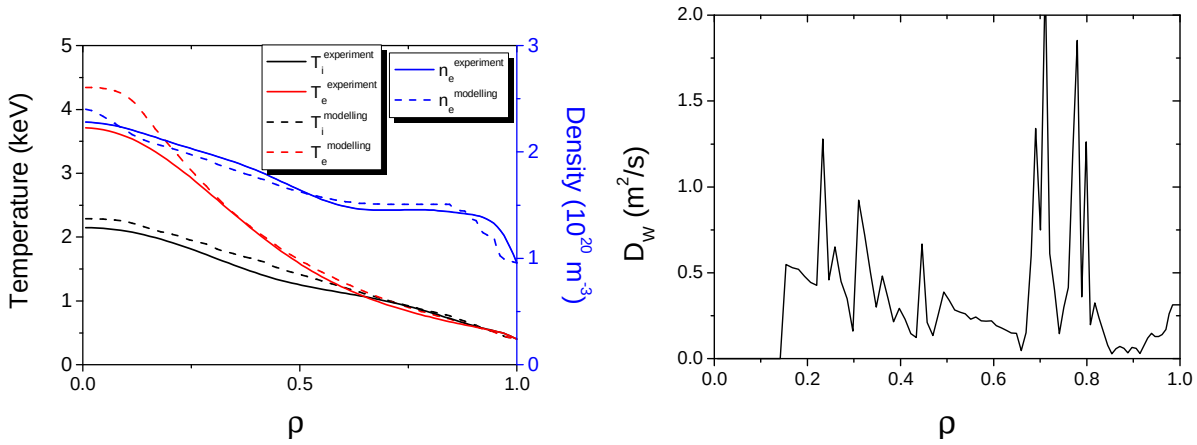

Figure 9. a) Alcator C-Mod experimental and ASTRA-modelled density and electron and ion temperature profiles versus normalized minor radius, with the same modelling assumptions as for ITER and with power deposition profiles evaluated from experimental measurements with TRANSP. b) Anomalous W diffusion coefficient predicted by GLF23 versus normalized minor radius for the simulations in a) with a region of suppressed anomalous transport near the plasma centre (up to $\rho = 0.15$) and with values in the range of 0.2 to 2.0 m^2/s for $\rho \geq 0.15$, which are similar to those required the experimental W emission temporal behaviour versus radius with STRAHL in Fig. 8.

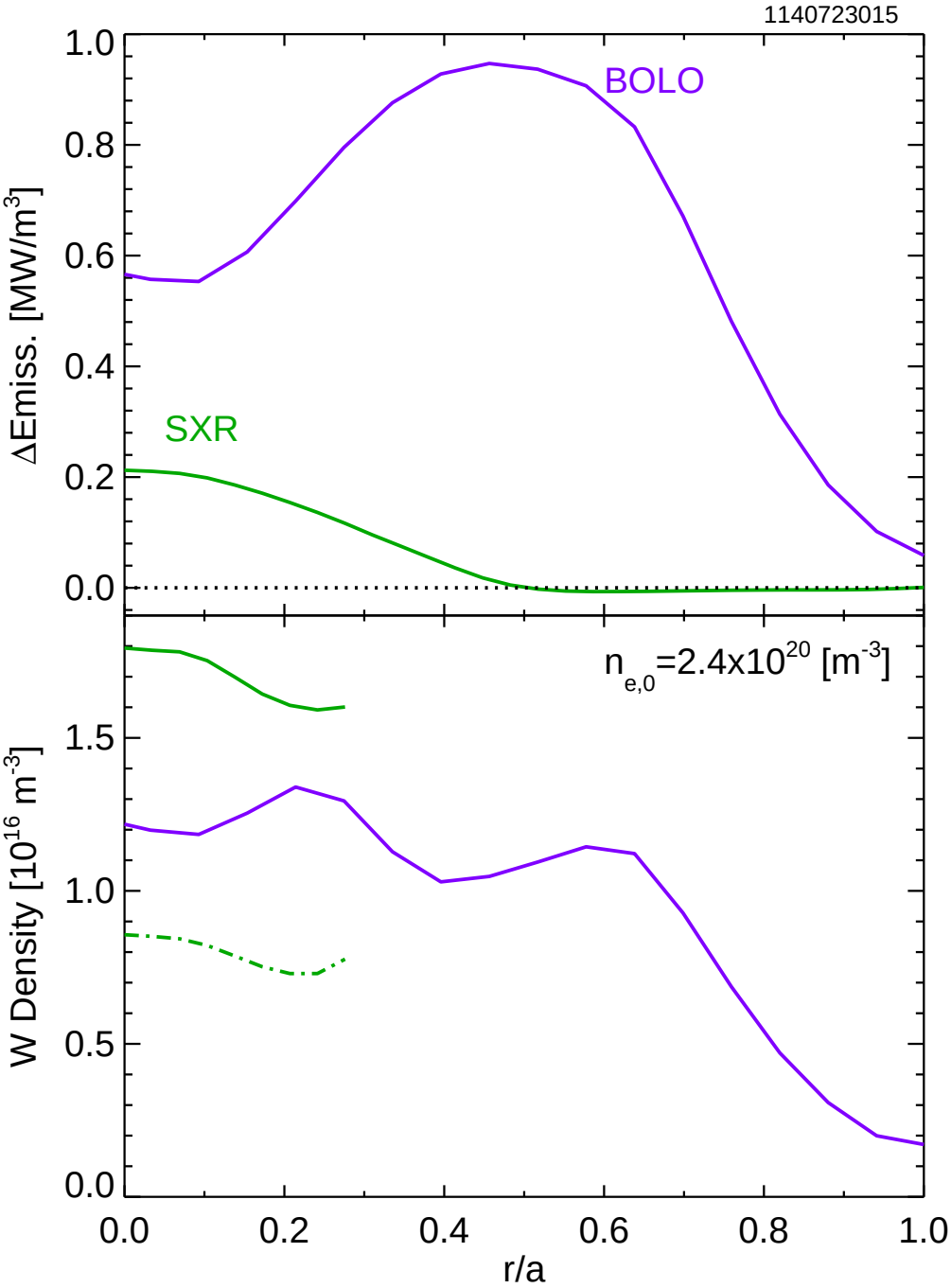

Figure 10. Top) Measurements of the increased radiated and soft X-ray power densities (through a 50 μm Be filter) following W LBO in an ITER-like Alcator C-Mod H-mode plasma. Bottom) Estimated W density from the radiated and soft X-ray power densities from the measured plasma density and temperature profiles and the expected radiation efficiency of W in these conditions. Full lines and dashed-lines correspond to estimates based on the different sets of atomic modelling data for the SXR emission.

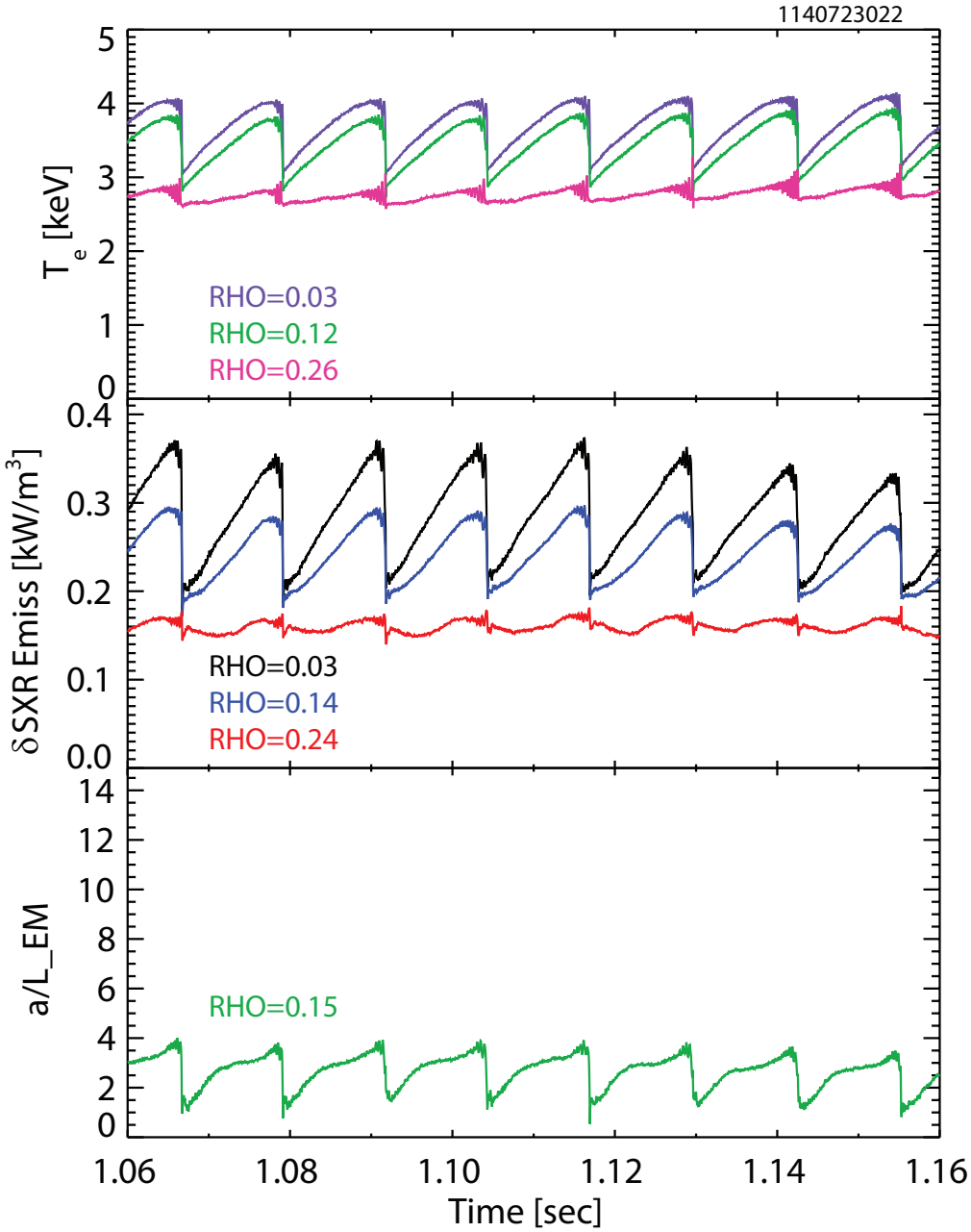

Figure 11. (Top) Measurements of the electron temperature evolution between sawteeth up to the inversion radius ($\rho \sim 0.25$) for an ITER-like H-mode plasma in Alcator C-Mod following W LBO injection. (Middle) Measurements of the soft X-ray power density (through a 50 μm Be filter) in an ITER-like Alcator C-Mod H-mode plasma following W LBO injection. (Bottom) Calculated emissivity gradient scale length at $\rho = 0.15$.

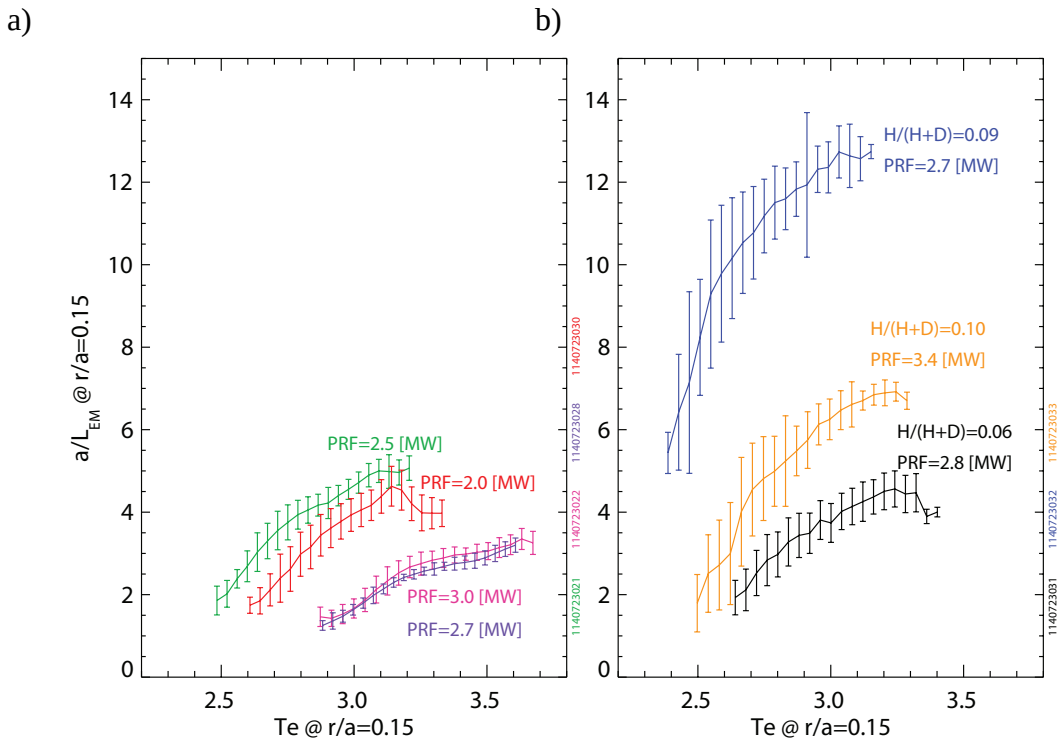

Figure 12. Measured scale length of the soft X-ray radiation at ρ = 0.15 evolving over the sawtooth cycle for a set of 0.52 MA ITER-like Alcator C-Mod H-mode plasmas: (a) ICRF power scan with no extrinsic H_2 puffing indicating a weak change in W peaking and (b) ICRF and H_2 scan showing a strong change in W peaking.

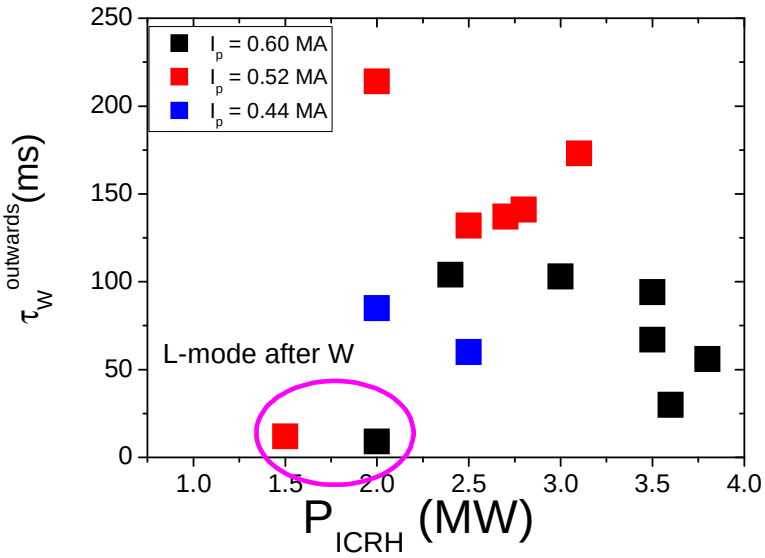

Figure 13. W confinement time versus coupled ICRH power for a set of the Alcator C-Mod ITER-like H-mode discharges. The points highlighted by a magenta circle correspond to discharges in which the W LBO triggers an H-L transition, as shown in Fig. 5.

Case	q_e^{α} (MWm^{-3})	q_i^{α} (MWm^{-3})	q_e^{RF} (MWm^{-3})	q_i^{RF} (MWm^{-3})
33 MW + 20 MW central ECRH	0.53	0.37	1.0	0
33 MW + 20 MW ICRH with He^3 minority	0.57	0.37	0.6	0.6

Table 1. Power densities deposited in the electron and ions by alpha heating at $\rho = 0$ for two ITER simulations with $Q_{DT} = 10$ and central RF heating (ECRH or ICRH He^3 minority).

Case	$T_e(\rho=0)/T_e(\rho=0.7)$	$T_i(\rho=0)/T_i(\rho=0.7)$	$n_e(\rho=0)/n_e(\rho=0.7)$	$n_i(\rho=0)/n_i(\rho=0.7)$
33 MW + 20 MW central ECRH	3.0	2.7	1.4	1.3
33 MW + 20 MW ICRH with He^3 minority	2.5	2.4	1.5	1.4
Alcator C-Mod P_{ICRH} = 3.0 MW	3.3	2.1	1.5	
Alcator C-Mod P_{ICRH} = 1.5 MW	3.6	2.8	1.3	

Table 2. Ratios of electron and ion temperatures and electron and ion densities at $\rho = 0$ and $\rho = 0.7$ for two ITER simulations with Q_{DT} =10 and 20 MW of central RF heating (ECRH or ICRH He^3 minority) and two Alcator C-Mod ITER-like H-mode discharges (those of Fig. 6) with two levels of ICRH power heating (1.5 and 3.0 MW).

T_e (ρ = 0.15)	a/L_{ne}	a/L_{Te}	$\frac{T_e}{L_W}\frac{dL_W}{dT_e}$	a/L_ε
2.5 keV	0.5	0-1.0	2.5-6.5	3.0-8.0
3.0 keV	0.5	0-1.0	2.2-2.7	2.7-4.2
3.5 keV	0.5	0-1.0	0.6-1.0	1.1-2.5
4.0 keV	0.5	0-1.0	0.0-0.7	0.5-2.2

Table 3. Inverse scale lengths for the electron density, temperature and normalized radiation efficiency at ρ =0.15 for a range of electron temperatures including their variation along the sawtooth cycle in Alcator C-Mod plasmas. The inverse scale length of the soft X-ray emission (a/L_ε) is evaluated from the values in this table and Eq. 5 assuming that $a/Ln_W = 0$.